

# Beyond Black & White: What Photospheric Magnetograms Can Teach Us About Solar Activity

Brian T. Welsch, Bill Abbett<sup>1</sup>, Dave Bercik<sup>1</sup>,

George H. Fisher<sup>1</sup>, Yan Li<sup>1</sup>, and Pete W. Schuck<sup>2</sup>

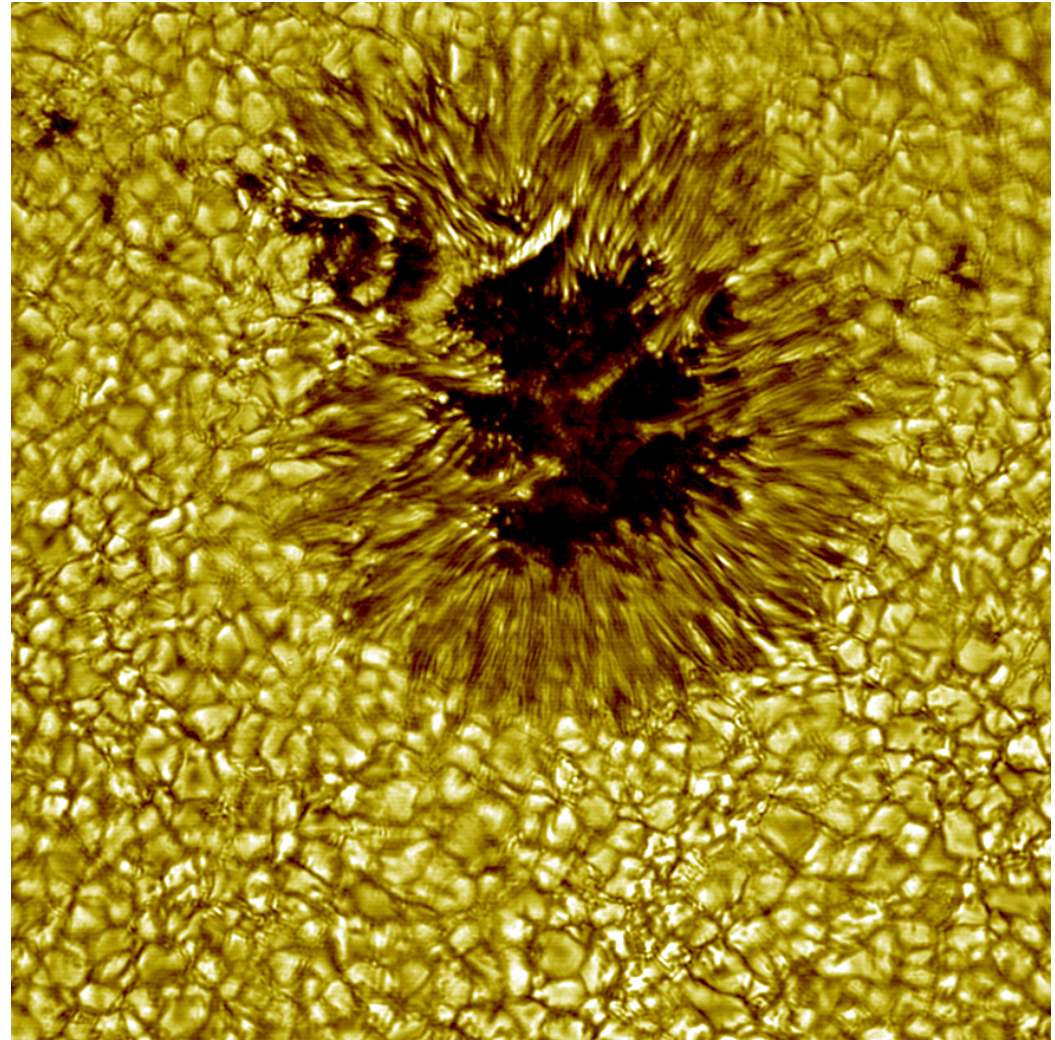
<sup>1</sup>*Space Sciences Lab, UC-Berkeley;* <sup>2</sup>*Space Weather Lab, NASA-GSFC*

Essentially all solar activity --- variations in the Sun's energetic output in the form of radiation, particles, and fields --- can be traced to the evolution of solar magnetic fields. Beyond the significant ramifications solar activity has for our society, its many facets are of great scientific interest. The magnetic fields that drive solar activity are generated within the Sun's interior, and can extend through the photosphere into the corona, coupling the Sun's interior with its outer atmosphere. Hence, measurements of magnetic fields at the photosphere can provide insights into magnetic evolution both in the interior and the outer atmosphere. While maps of the photospheric magnetic field --- magnetograms --- have been produced routinely for decades, the cadence and quality of such measurements has improved dramatically in recent years, providing new insights into many aspects of the Sun's rich magnetic variability. I will present recent studies undertaken by myself and collaborators that use magnetograms to understand magnetic evolution over spatial scales ranging from granules to active regions, with implications for several aspects solar activity, including dynamo processes on small and large scales, and impulsive events such as flares and CMEs.

Observations of spots on the surface of the Sun were probably the first indications that it is an active star.

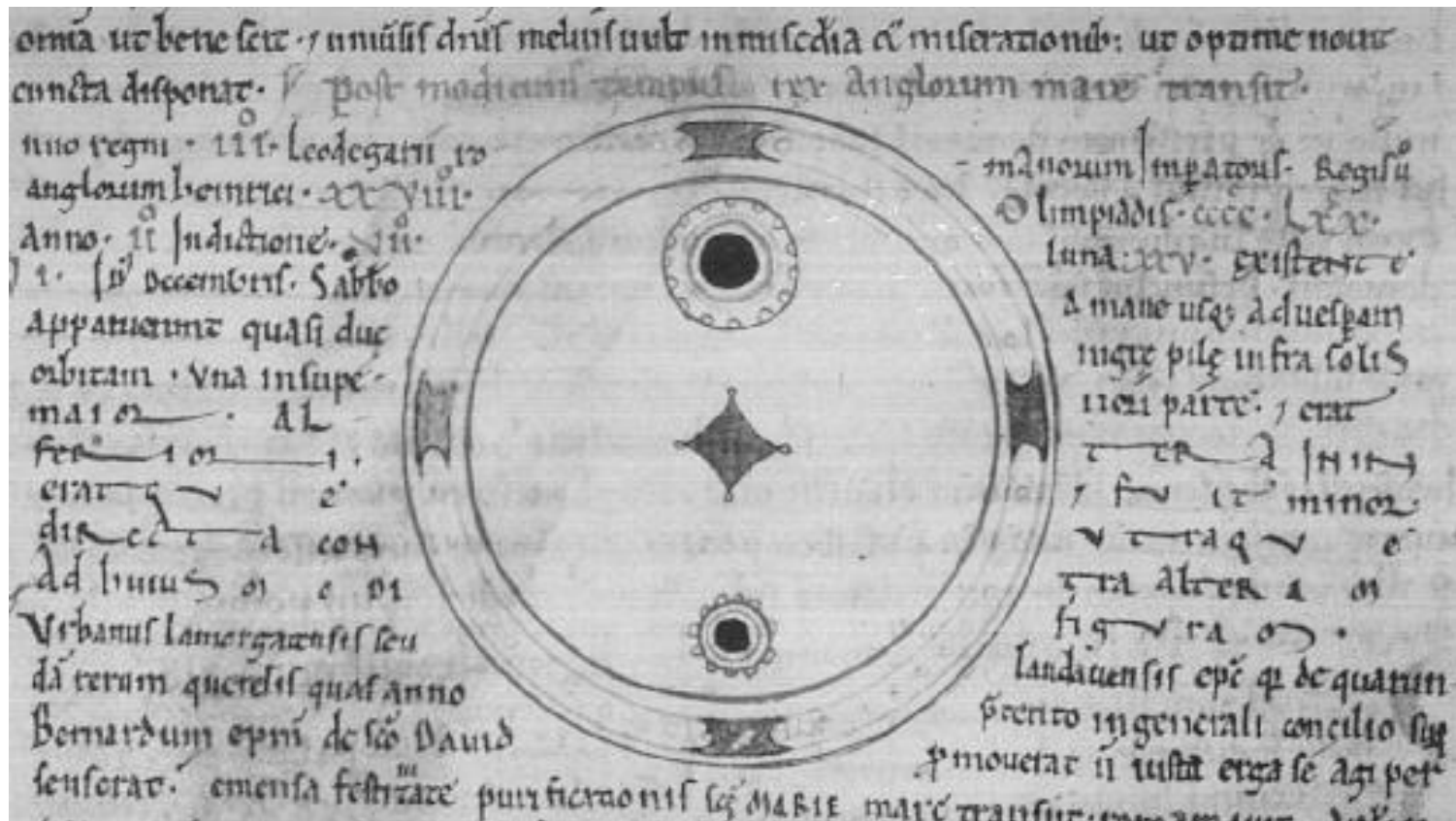
Records of naked-eye sunspot observations date back more than 2000 years.

This Dunn Solar Telescope image shows a sunspot in visible light.



[National Solar Observatory/AURA/NSF](#)

Perhaps the oldest reproduction of a sunspot --- a drawing --- dates from the 12<sup>th</sup> century.



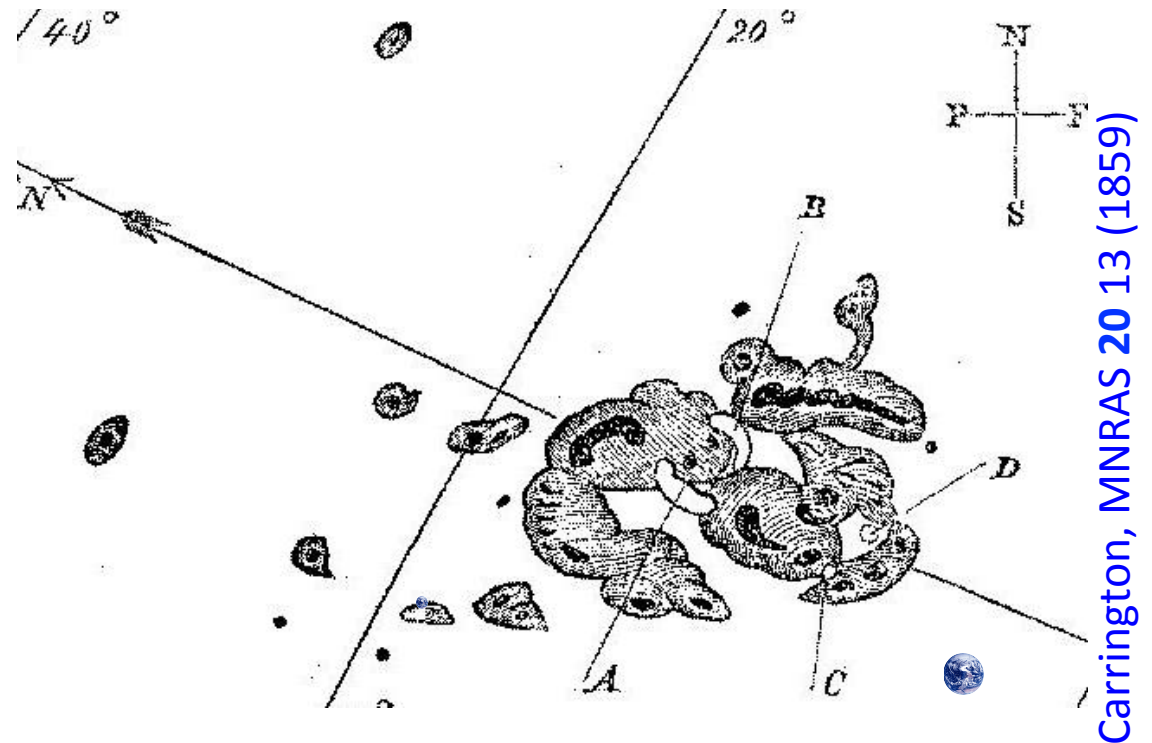
From “the Chronicles of John of Worcester, twelfth century. Notice the depiction of the penumbra around each spot. Reproduced from R.W. Southern, Medieval Humanism, Harper & Row 1970, [Plate VII].”

[http://www.astro.umontreal.ca/~paulchar/grps/histoire/newsite/sp/great\\_moments\\_e.html](http://www.astro.umontreal.ca/~paulchar/grps/histoire/newsite/sp/great_moments_e.html)

Long before physics could explain it, a solar-terrestrial connection related to sunspots was identified.

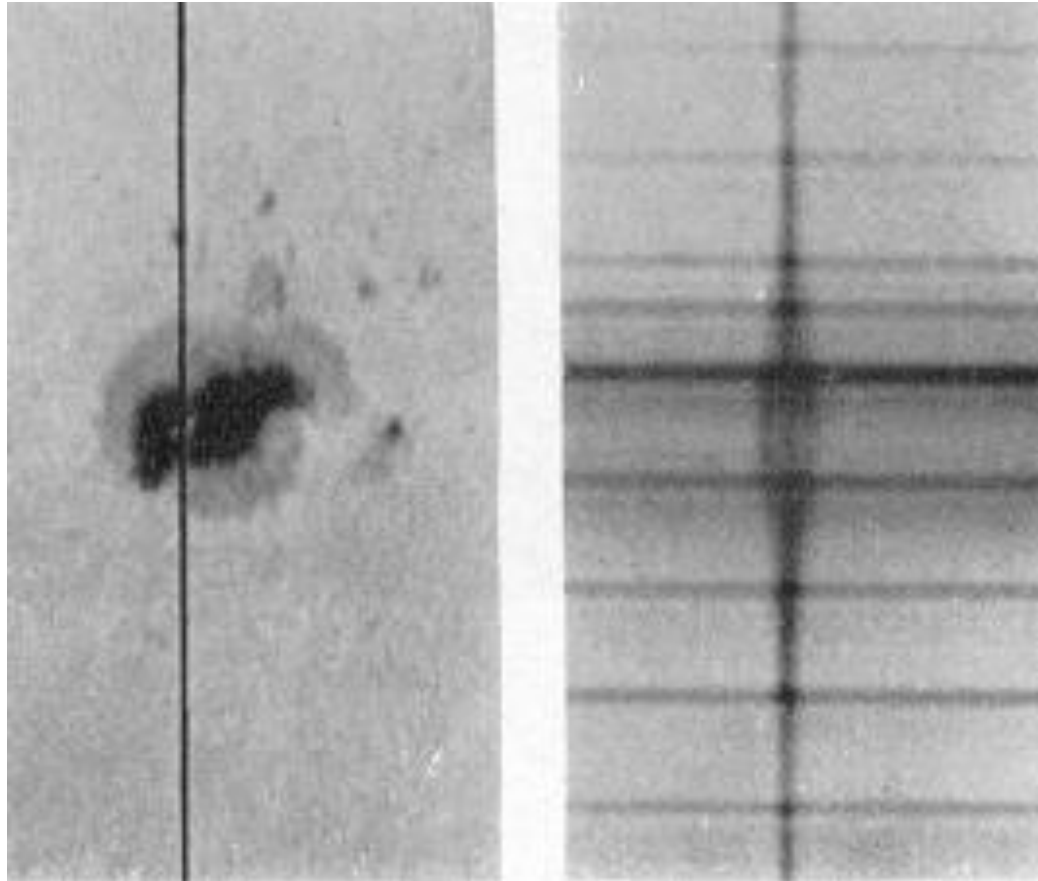
- In 1852, Sabine, Wolf, Gautier, and Lamont independently recognized that Schwabe's sunspot cycles coincided with cycles of geomagnetic variability.

- In 1859, shortly after Carrington made the first recorded observation of a solar flare (right), terrestrial magnetic variations and low-latitude aurorae were noted.



Note two pairs of bright features, A & B (“ribbons”) and C

In 1907-8, Hale et al. showed that sunspots were magnetic --- rescuing the Sun from certain astronomical obscurity!

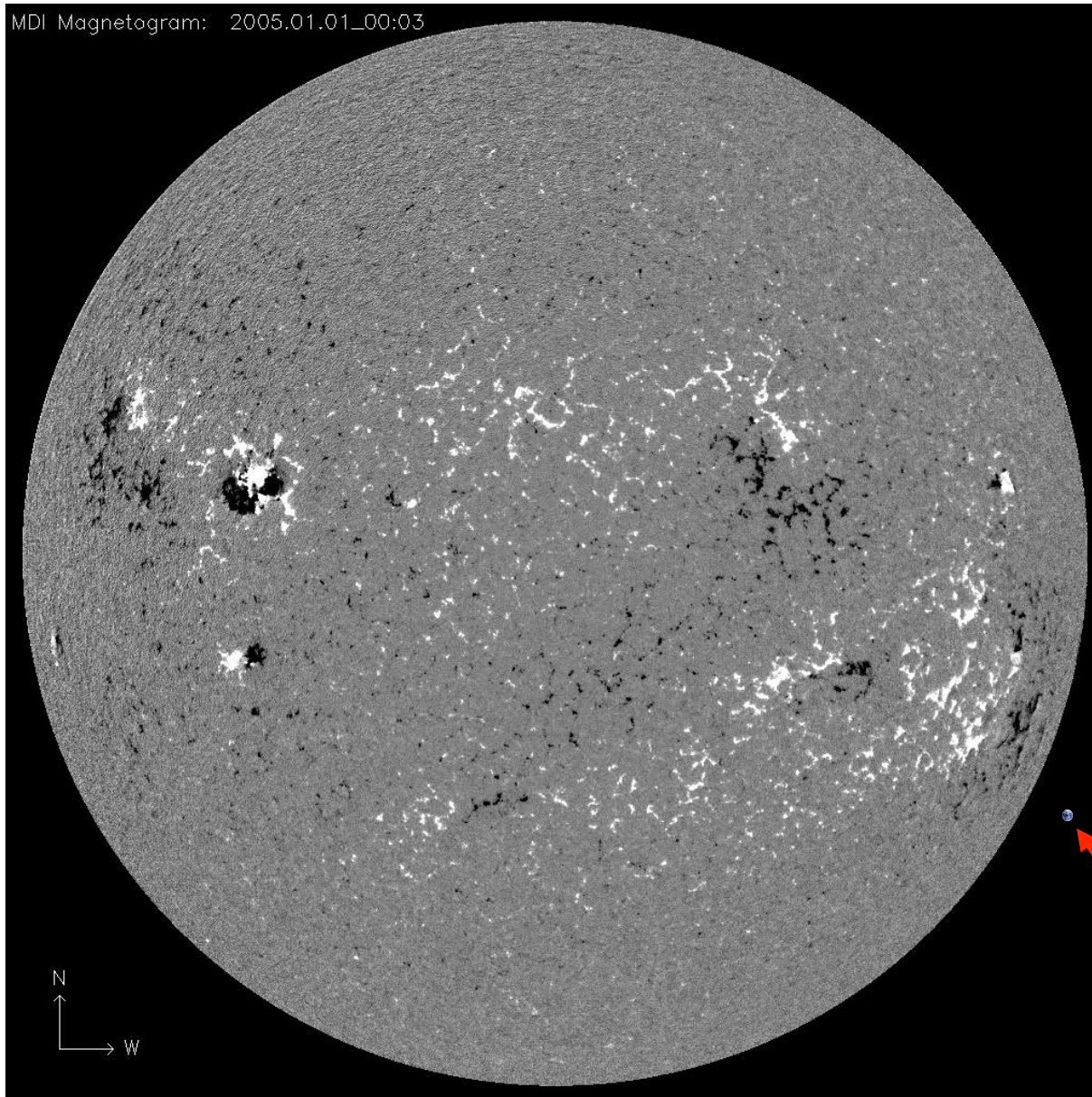


Hale et al. ApJ 49 153 (1919)  
Image Credit: P. Charbonneau

*“Magnetic fields are to astrophysics as sex is to psychology.”*

– H.C. van der Hulst, 1987

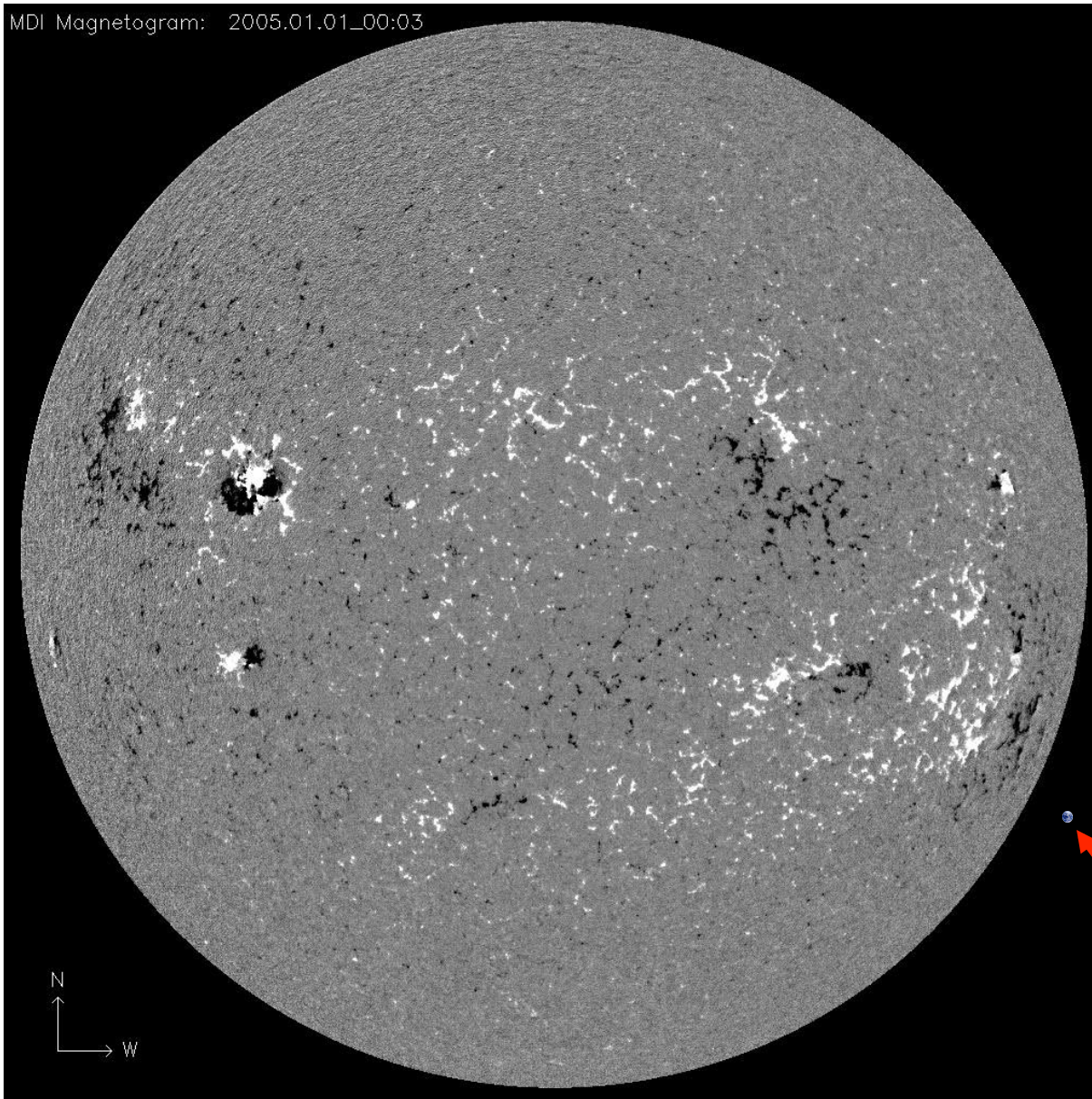
We now know the Sun's photosphere teems with magnetic activity on all observable scales.



These MDI full-disk, line-of-sight magnetograms show emergence and evolution in active regions and smaller scale fields during January 2005.

Note Earth, shown for scale.

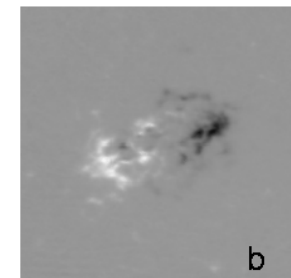
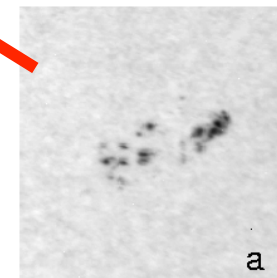
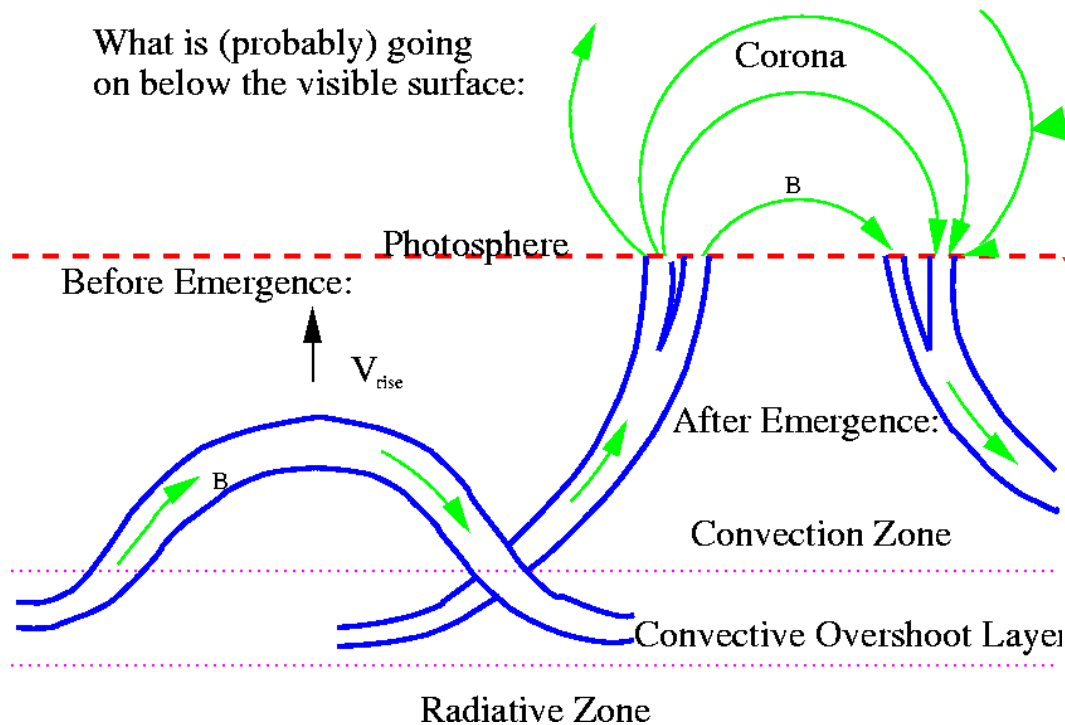
Observations show that the Sun's photosphere teems with magnetic activity on all observable scales.



These MDI full-disk, line-of-sight magnetograms show emergence and evolution in active regions and smaller scale fields during January 2005.

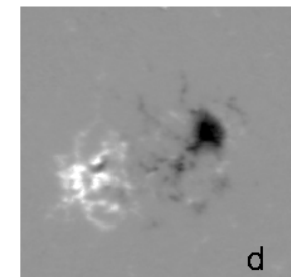
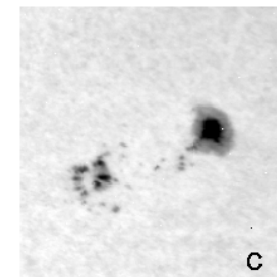
Note Earth, shown for scale.

Surface magnetism is seen as one manifestation of structures extending from the interior into the corona.



NOAA 7624 93-11-30 N03 W12

N  
W



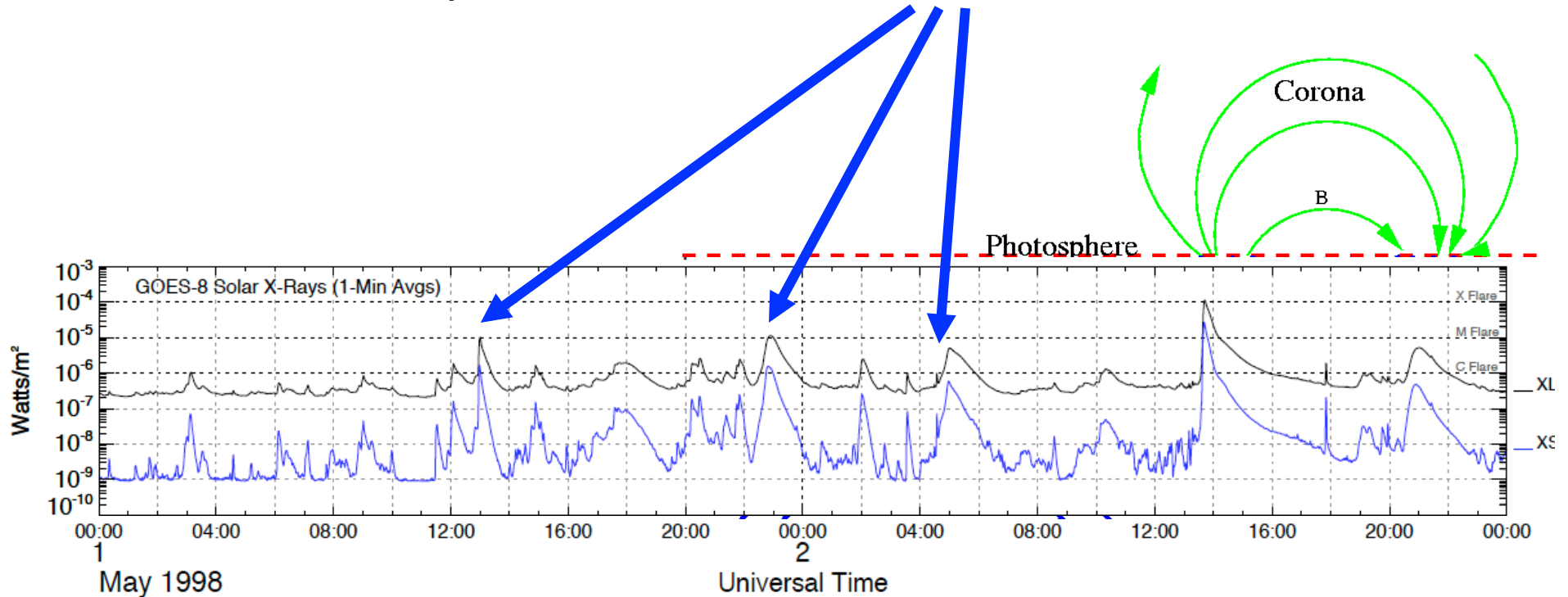
NOAA 7624 93-12-01 N03 W26

700  
0 G  
-1000

Image credits: George Fisher, LMSAL/TRACE

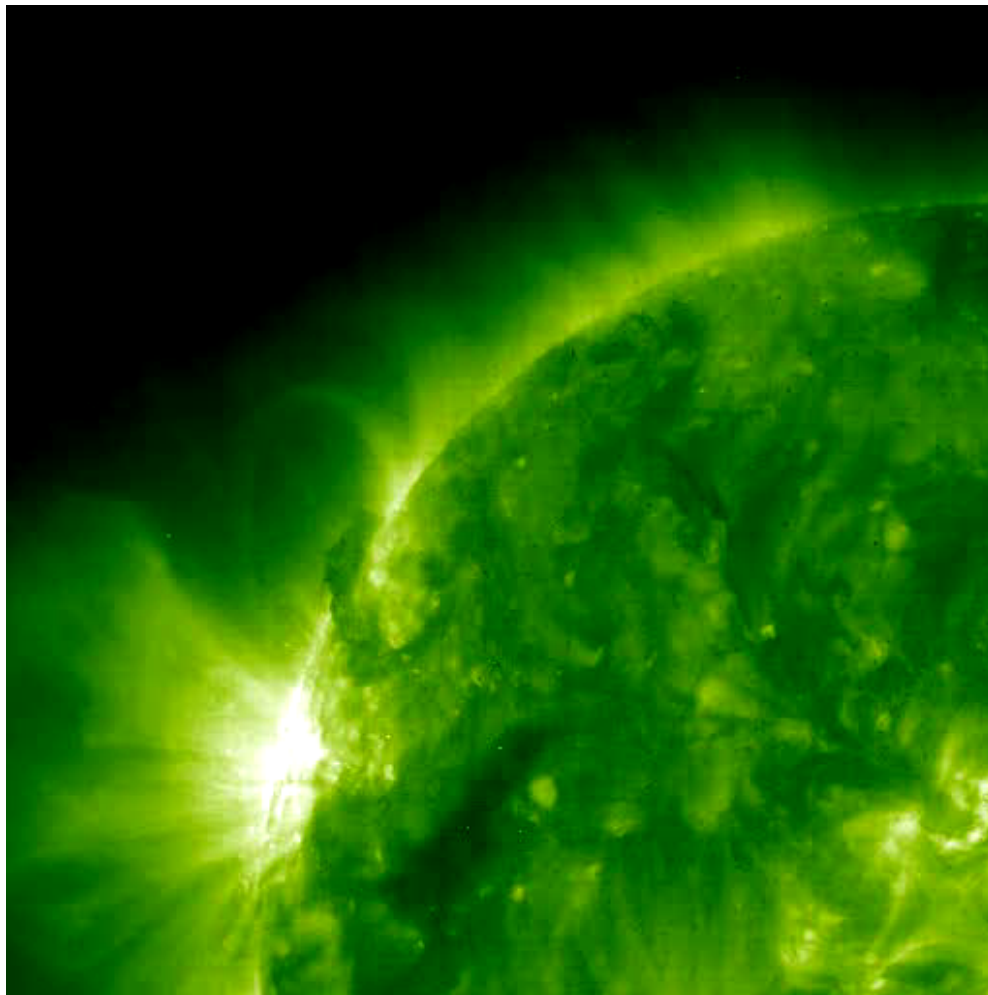
Evidently, observations of magnetism at the Sun's surface have a long history in the study of solar activity!

In this vein, today I'll discuss how **photospheric** magnetic evolution can help us understand **flares** in the **corona**.



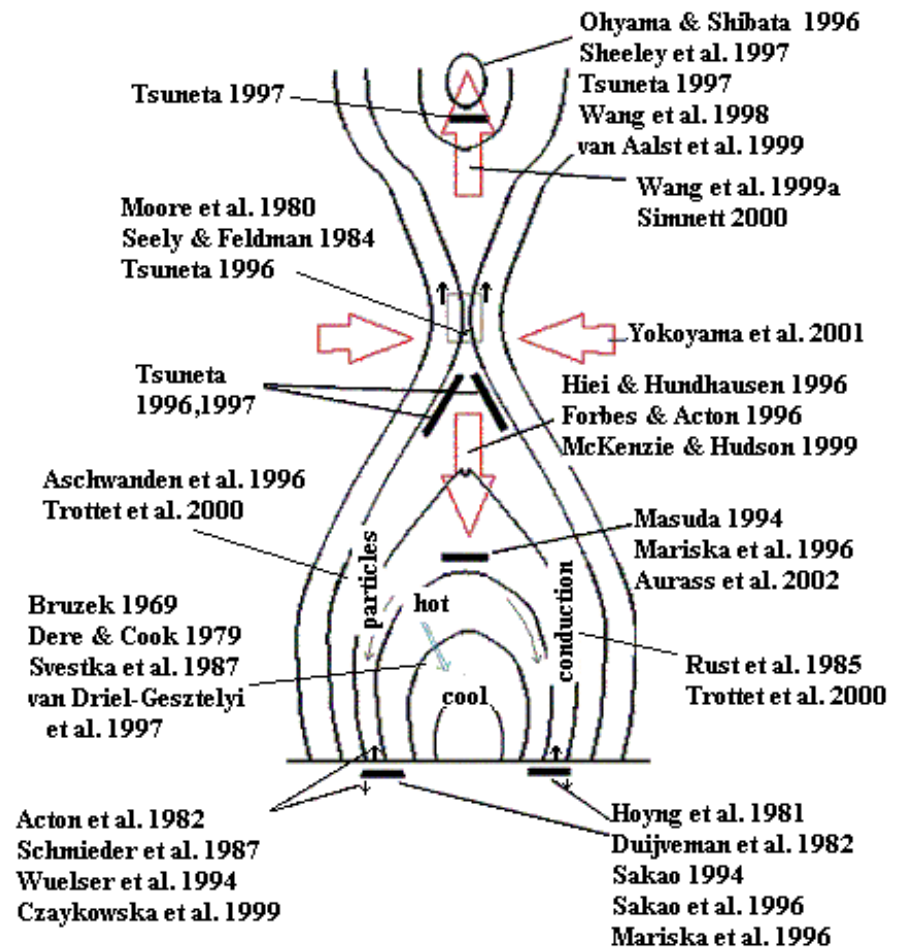
Flares are driven by the release of energy stored in electric currents in the coronal magnetic field.

an EUV movie of  $\sim 1.5\text{MK}$  thermal emission



Movie credit: SOHO/EIT team

the “standard model”



McKenzie 2002

# Flares and CMEs are powered by energy in the coronal magnetic field.

**Table 1.** Energy Requirements for a Moderately Large CME

Parameter	Value
Kinetic energy (CME, prominence, and shock)	$10^{32}$ ergs
Heating and radiation	$10^{32}$ ergs
Work done against gravity	$10^{31}$ ergs
Volume involved	$10^{30}$ cm <sup>3</sup>
Energy density	100 ergs cm <sup>-3</sup>

**Table 2.** Estimates of Coronal Energy Sources

Form of Energy	Observed Average Values	Energy Density ergs cm <sup>-3</sup>
Kinetic ( $(m_p n V^2)/2$ )	$n = 10^9$ cm <sup>-3</sup> , $V = 1$ km s <sup>-1</sup>	$10^{-5}$
Thermal ( $nkT$ )	$T = 10^6$ K	0.1
Gravitational ( $m_p n g h$ )	$h = 10^5$ km	0.5
Magnetic ( $B^2/8\pi$ )	$B = 100$ G	400

From T.G. Forbes, "A Review on the Genesis of Coronal Mass Ejections", JGR (2000)

While flares are driven by the coronal field  $\mathbf{B}_{\text{cor}}$ , studying the photospheric field  $\mathbf{B}_{\text{ph}}$  is essential.

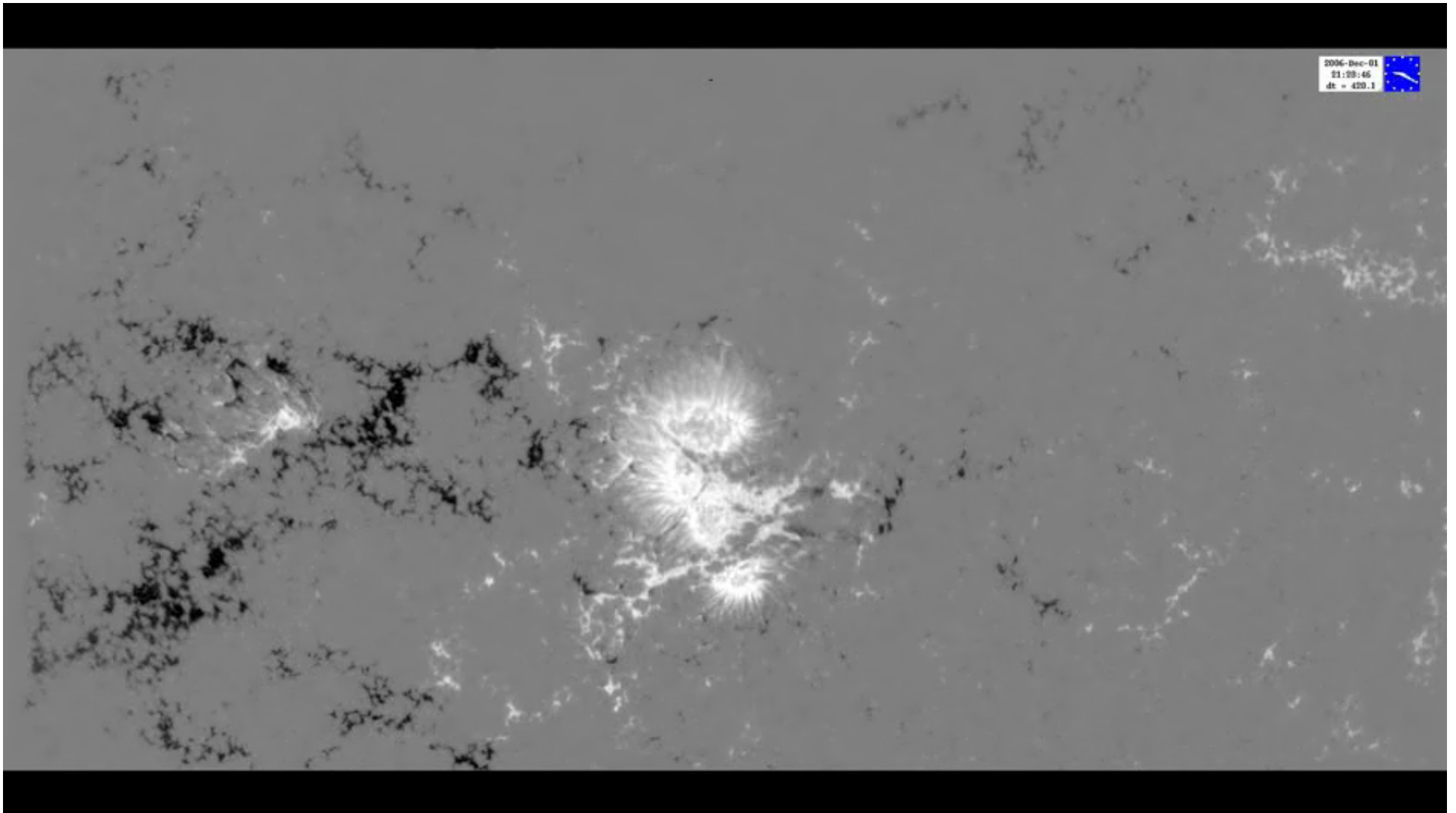
Coronal electric currents cannot (currently) be measured: measurements of (vector)  $\mathbf{B}_{\text{cor}}$  are rare and uncertain.

When not flaring, coronal magnetic evolution should be nearly ideal ==> **magnetic connectivity is preserved.**

While  $\mathbf{B}_{\text{cor}}$  can evolve on its own, changes in the photospheric field  $\mathbf{B}_{\text{ph}}$  will induce changes in the coronal field  $\mathbf{B}_{\text{cor}}$ .

In addition, following active region (AR) fields in time can provide information about their **history** and **development.**

Fundamentally, the photospheric field is the “source” of the coronal field; the two regions are magnetically coupled.



Credit: Hinode/SOT Team; LMSAL, NASA

What physical processes produce the electric currents that store energy in  $\mathbf{B}_{\text{cor}}$ ? Two options are:

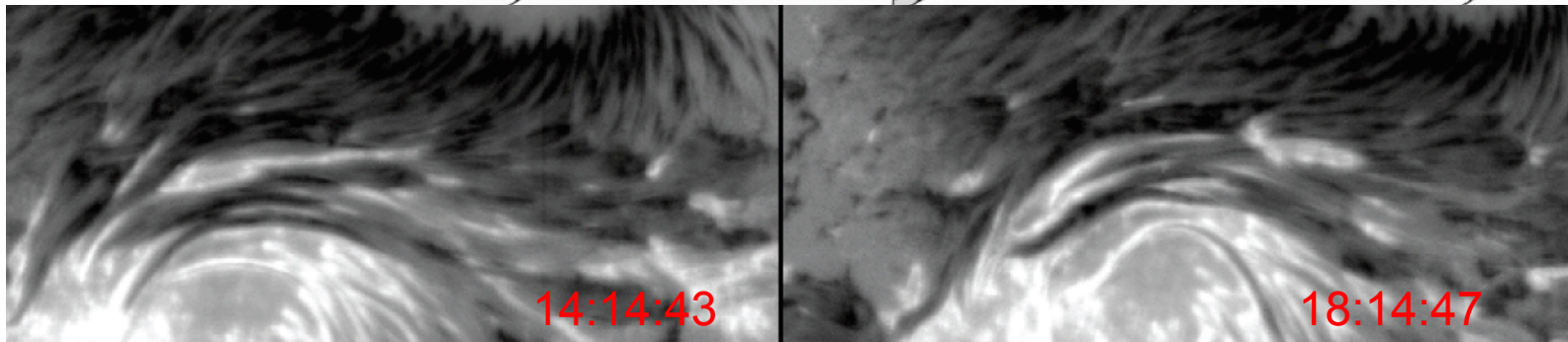
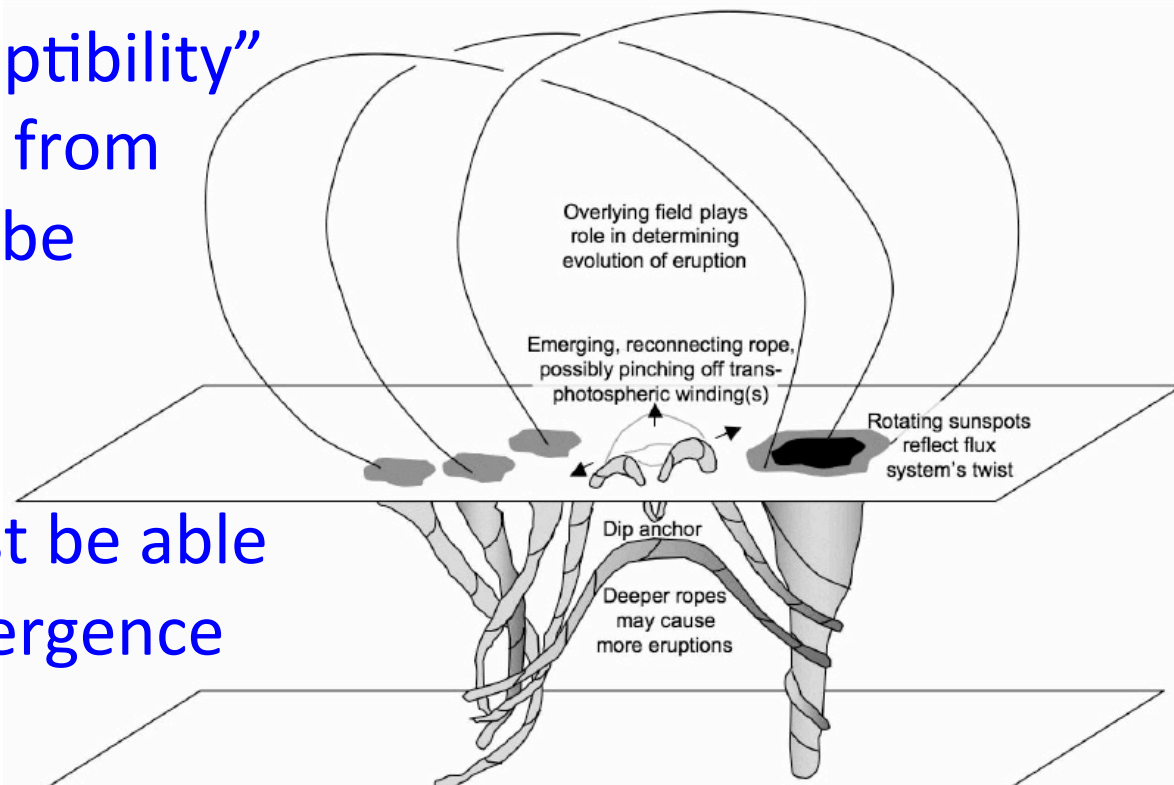
- Currents could form in the interior, then emerge into the corona.
  - Current-carrying magnetic fields have been observed to emerge (e.g., Leka et al. 1996, Okamoto et al. 2008).
- Photospheric evolution could induce currents in already-emerged coronal magnetic fields.
  - From simple scalings, McClymont & Fisher (1989) argued induced currents would be too weak to power large flares.
  - Detailed studies by Longcope et al. (2007) and Kazachenko et al. (2009) suggest strong enough currents can be induced.

*Both models involve slow buildup, then sudden release.*

If the currents that drive flares and CMEs form in the interior, then to understand and predict these:

1) Coronal “susceptibility” to destabilization from emergence must be understood;

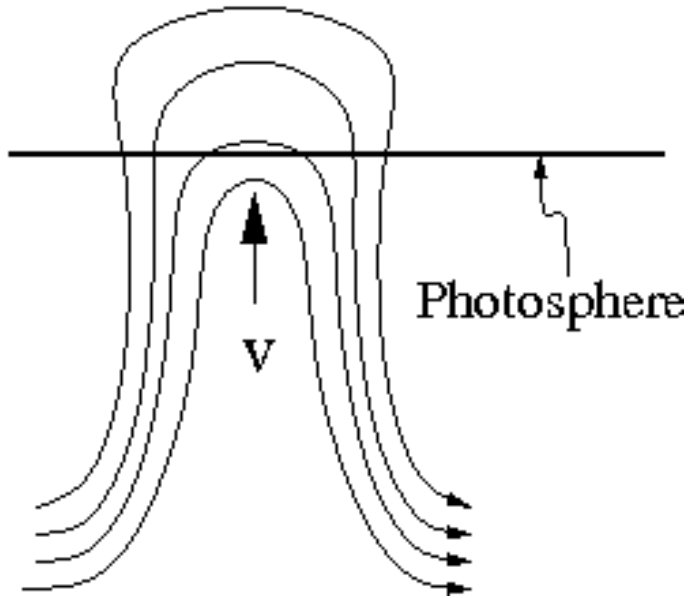
2) Observers must be able to detect the emergence of new flux!



Schrijver et al., ApJ v. 675 p. 1637 2008,  
Schrijver ASR v. 43 p. 789 2009

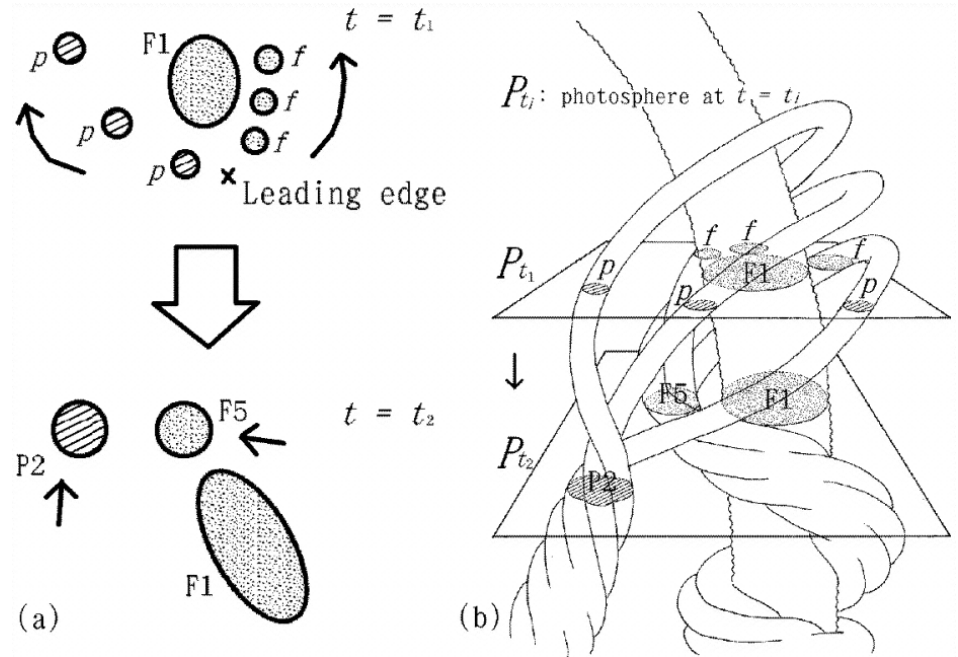
**Note:** Currents can emerge in two distinct ways!

a) emergence of new flux



NB: New flux only emerges along polarity inversion lines!

b) vertical transport of currents in emerged flux

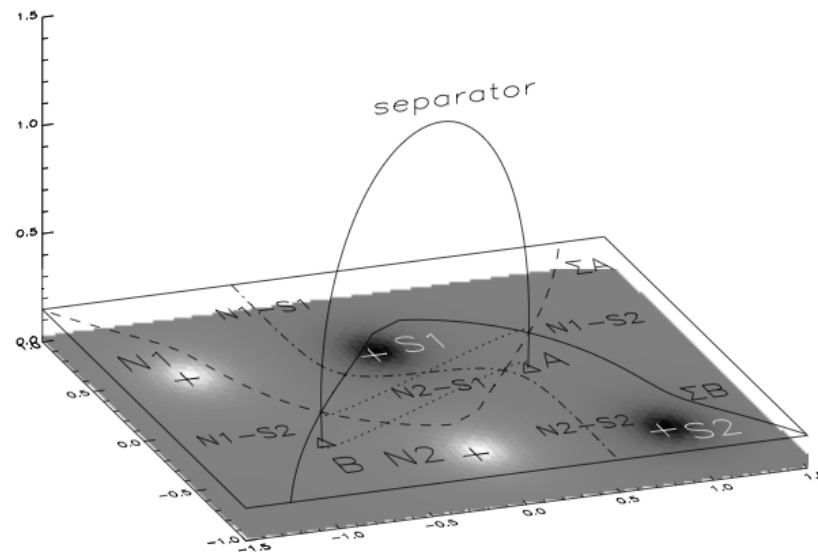
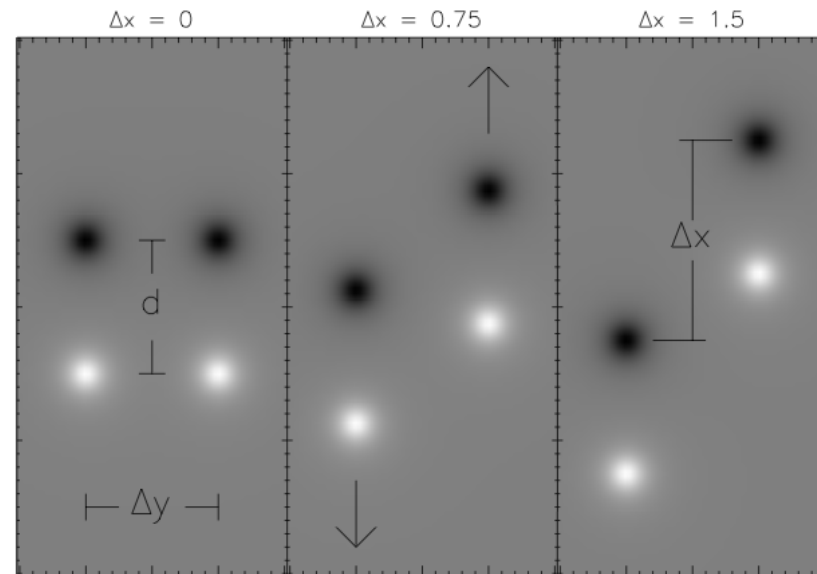


NB: This does not increase total unsigned photospheric flux.

If coronal currents induced by post-emergence photospheric evolution drive flares and CMEs, then:

The evolving coronal magnetic field must be modeled!

NB: Induced currents close along or above the photosphere --- they are not driven from below.



An electric field  $\mathbf{E}$  derived from magnetogram evolution can quantify aspects of evolution in  $\mathbf{B}_{\text{cor}}$ .

- The fluxes of magnetic energy & helicity across the magnetogram surface into the corona depend upon  $\mathbf{E}$ :

$$dU/dt = \int dA (\mathbf{E} \times \mathbf{B})_z / 4\pi$$

$$dH/dt = 2 \int dA (\mathbf{E} \times \mathbf{A})_z$$

$U$  and  $H$  probably play central roles in flares / CMEs.

- Coupling of  $\mathbf{B}_{\text{cor}}$  to  $\mathbf{B}$  beneath the corona implies estimates of  $\mathbf{E}$  there provide boundary conditions for data-driven, time-dependent simulations of  $\mathbf{B}_{\text{cor}}$ .

# The hypothetical coronal magnetic field with lowest energy is current-free, or “potential.”

- For a given coronal field  $\mathbf{B}_C$ , the coronal magnetic energy is:

$$U \equiv \int dV (\mathbf{B}_C \cdot \mathbf{B}_C)/8\pi.$$

- The lowest energy coronal field would have current  $\mathbf{J} = 0$ , and Ampère says  $4\pi\mathbf{J}/c = \nabla \times \mathbf{B}$ , so  $\nabla \times \mathbf{B}_{\min} = 0$ .
- A curl-free vector field can be expressed as the gradient of a scalar potential,  $\mathbf{B}_{\min} = -\nabla\chi$ . (Since  $\nabla^2\chi = 0$ , use electrostatics to solve!)

$$U_{\min} \equiv \int dV (\mathbf{B}_{\min} \cdot \mathbf{B}_{\min})/8\pi$$

- The difference  $U^{(F)} = [U - U_{\min}]$  is “free” energy stored in the corona, which can be suddenly released in flares or CMEs.

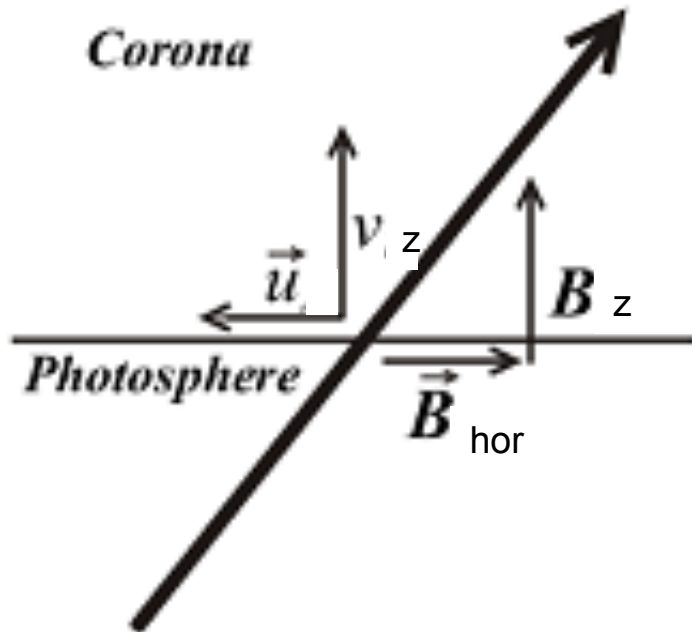
Assuming  $\mathbf{B}_{\text{ph}}$  evolves ideally (e.g., Parker 1984), then photospheric flow and magnetic fields are coupled.

- The magnetic induction equation's  $\mathbf{z}$ -component relates the flux transport velocity  $\mathbf{u}$  to  $dB_z/dt$  (Demoulin & Berger 2003):

$$\Delta B_z / \Delta t = -c [ \nabla \times \mathbf{E} ]_z = [ \nabla \times (\mathbf{v} \times \mathbf{B}) ]_z = - \nabla \cdot (\mathbf{u} B_z)$$

- Many tracking (“optical flow”) methods to estimate the  $\mathbf{u}$  have been developed, e.g., LCT (November & Simon 1988), FLCT (Fisher & Welsch 2008), DAVE (Schuck 2006).
- Purely numerical “inductive” techniques have also been developed (Longcope 2004; Fisher et al. 2010).

The apparent motion of magnetic flux in magnetograms is the **flux transport velocity,  $\mathbf{u}$** .



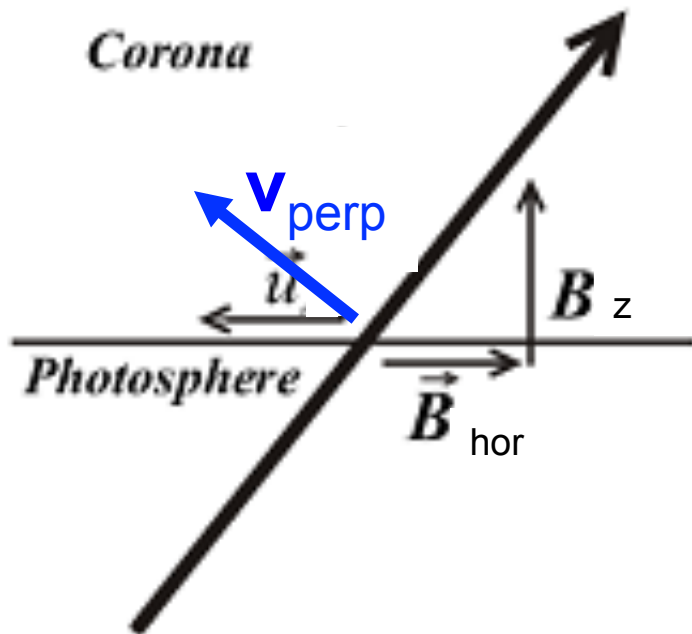
Démoulin & Berger (2003):  
In addition to horizontal flows, vertical velocities can lead to  $\mathbf{u} \neq 0$ . In this figure,  $\mathbf{v}_{hor} = 0$ , but  $v_z \neq 0$ , so  $\mathbf{u} \neq 0$ .

$\mathbf{u}$  is **not** equivalent to  $\mathbf{v}$ ; rather,  $\mathbf{u} \equiv \mathbf{v}_{hor} - (v_z/B_z)\mathbf{B}_{hor}$

- $\mathbf{u}$  is the apparent velocity (2 components)
- $\mathbf{v}$  is the actual plasma velocity (3 components)

(NB: non-ideal effects can also cause flux transport!)

The apparent motion of magnetic flux in magnetograms is the **flux transport velocity,  $\mathbf{u}$** .



Démoulin & Berger (2003) didn't use the fact that only the components of  $\mathbf{v}$  perpendicular to  $\mathbf{B}$  can change  $\mathbf{B}$ . Hence, one can ignore the comp. of  $\mathbf{v}$  along  $\mathbf{B}$ .

$\mathbf{u}$  is **not** equivalent to  $\mathbf{v}$ ; rather,  $\mathbf{u} \equiv \mathbf{v}_{\text{hor}} - (v_z/B_z)\mathbf{B}_{\text{hor}}$

- $\mathbf{u}$  is the apparent velocity (2 components)
- $\mathbf{v}_{\text{perp}}$  is the perpendicular plasma velocity (2 comps)

(NB: non-ideal effects can also cause flux transport!)

We studied flows  $\{\mathbf{u}\}$  from MDI magnetograms and flares from GOES for a few dozen active region (ARs).

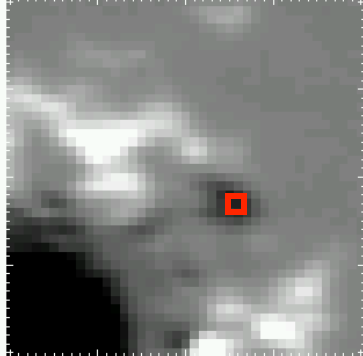
- $N_{\text{AR}} = 46$  ARs from 1996-1998 were selected.
- $> 2500$  MDI full-disk, 96-minute cadence, line-of-sight magnetograms were compiled.
- We estimated flows in these magnetograms using two separate tracking methods, FLCT and DAVE.
- The GOES soft X-ray flare catalog was used to determine source ARs for flares at and above C1.0 level.

## Magnetogram Data Handling

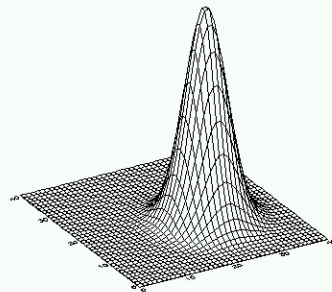
- Pixels  $> 45^\circ$  from disk center were not tracked.
- To estimate the radial field, cosine corrections were used,  $B_R = B_{LOS}/\cos(\Theta)$ . [dirty laundry!]
- Mercator projections were used to conformally map the irregularly gridded  $B_R(\vartheta, \varphi)$  to a regularly gridded  $B_R(x, y)$ .
- Corrections for scale distortion were applied.

Fourier local correlation tracking (FLCT) finds  $\mathbf{u}(x, y)$  by correlating subregions, to find local shifts.

AR 8210 (VM), 1998/05/01, 17:13

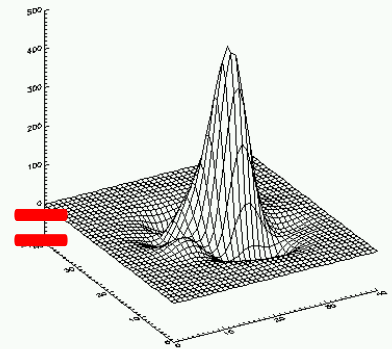
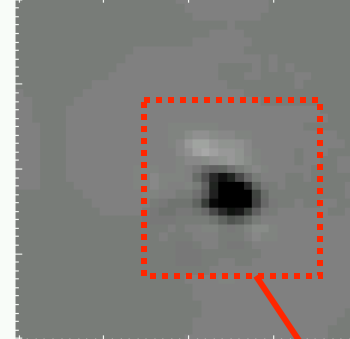


×

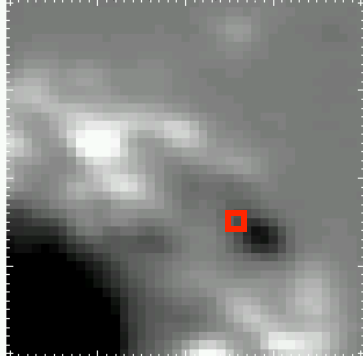


=

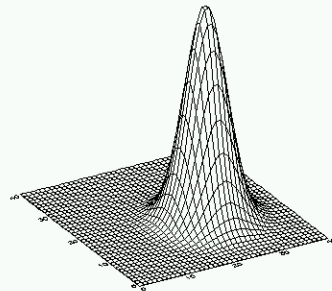
Masked Image 1



AR 8210 (VM), 1998/05/01, 21:29

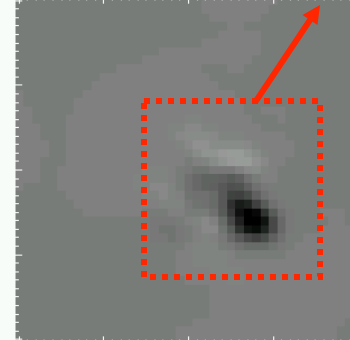


×



=

Masked Image 2



\*

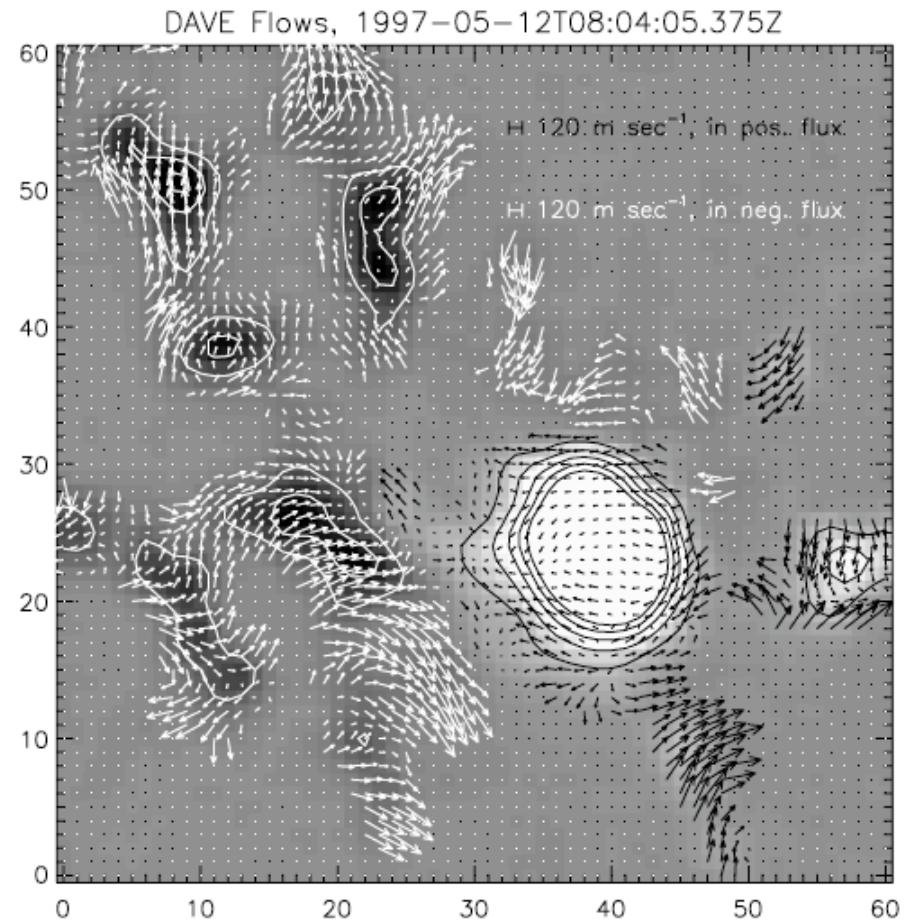
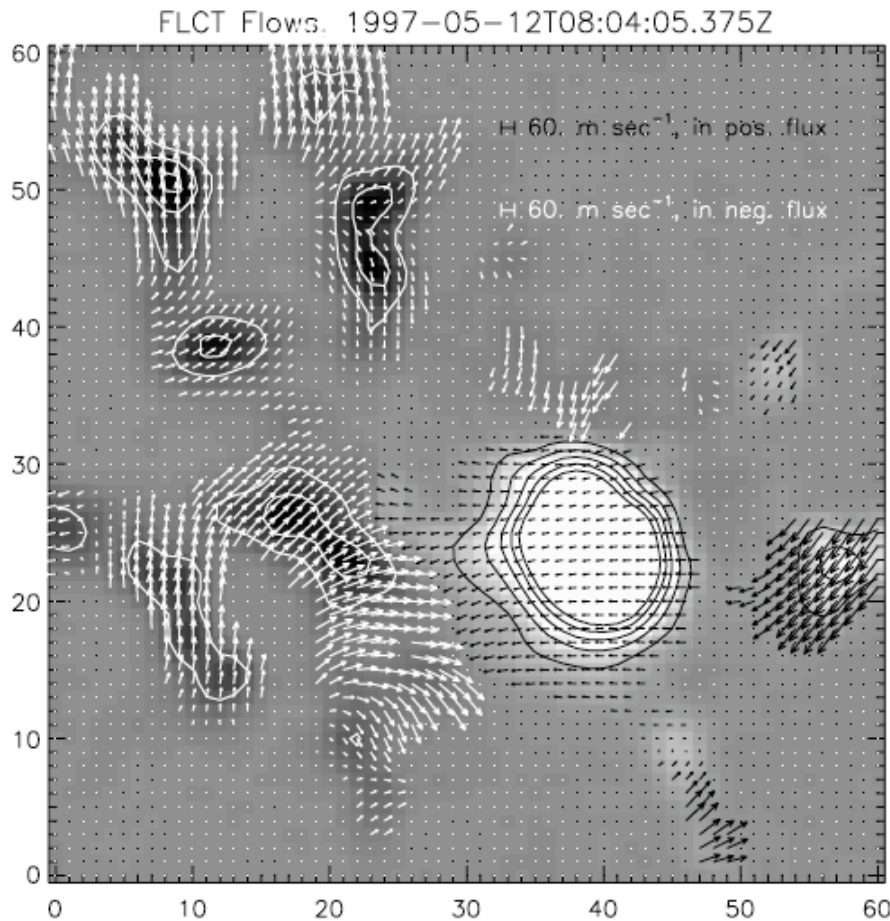
1) for ea.  $(x_i, y_i)$  above  $|B|_{\text{threshold}}$

2) apply Gaussian mask at  $(x_i, y_i)$

3) truncate and cross-correlate

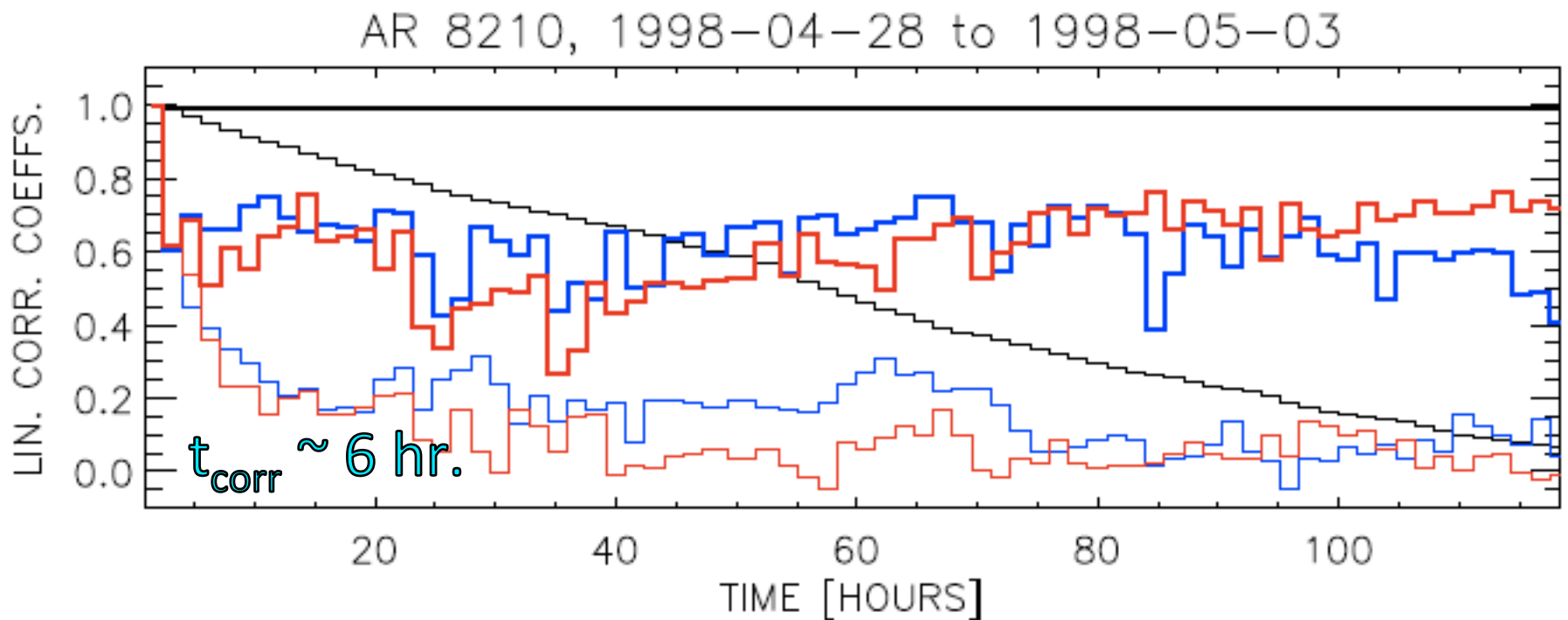
4)  $\Delta \mathbf{x}(x_i, y_i)$  is interpolated max. of correlation funct

Sample maps of FLCT and DAVE flows show them to be strongly correlated, but far from identical.



When weighted by the estimated radial field  $|B_R|$ , the FLCT-DAVE correlations of flow components were  $> 0.7$ .

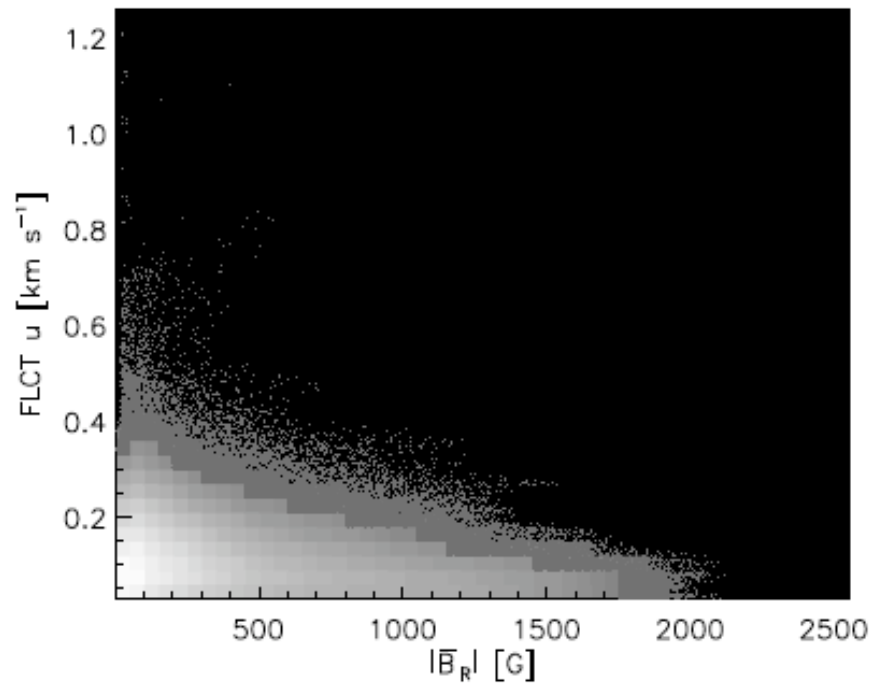
Autocorrelation of  $u_x$  and  $u_y$  suggest the 96 minutes cadence for magnetograms is not unreasonably slow.



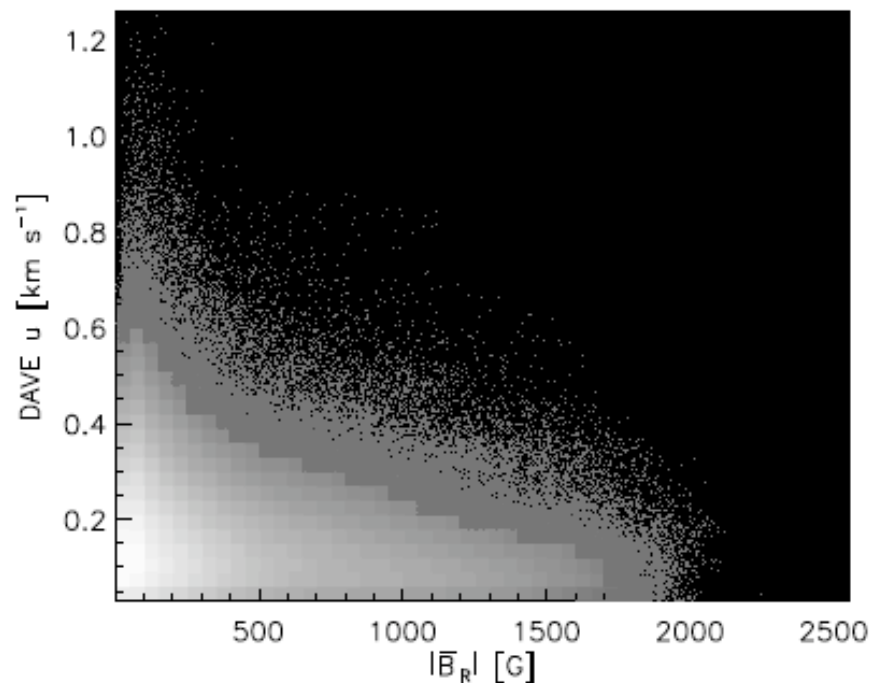
BLACK shows autocorrelation for  $B_R$ ; **thick** is current-to-previous, thin is current-to-initial.

BLUE shows autocorrelation for  $u_x$ ; **thick** is current-to-previous, thin is current-to-initial.

RED shows autocorrelation for  $u_y$ ; **thick** is current-to-previous, thin is current-to-initial.



For both FLCT and DAVE flows, speeds  $\{u\}$  were not strongly correlated with  $B_R$  --- rank-order correlations were 0.07 and -0.02, respectively.



The highest speeds were found in weak-field pixels, but a range of speeds were found at each  $B_R$ .

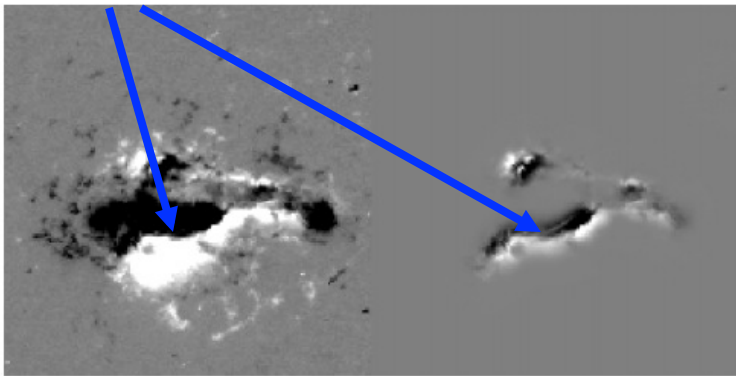
For each estimated radial magnetic field  $B_R(x,y)$  and flow  $\mathbf{u}(x,y)$ , we computed several properties, e.g.,

- average unsigned field  $|B_R|$
- summed unsigned flux,  $\Phi = \Sigma |B_R| da^2$
- summed flux near strong-field PILs,  $R$  (Schrijver 2007)
- sum of field squared,  $\Sigma B_R^2$
- rates of change  $d\Phi/dt$  and  $dR/dt$
- summed speed,  $\Sigma u$ .
- averages and sums of divergences  $(\nabla_h \cdot \mathbf{u})$ ,  $(\nabla_h \cdot \mathbf{u} B_R)$
- averages and sums of curls  $(\nabla_h \times \mathbf{u})$ ,  $(\nabla_h \times \mathbf{u} B_R)$
- the summed “proxy Poynting flux,”  $S_R = \Sigma u B_R^2$

(and many more!)

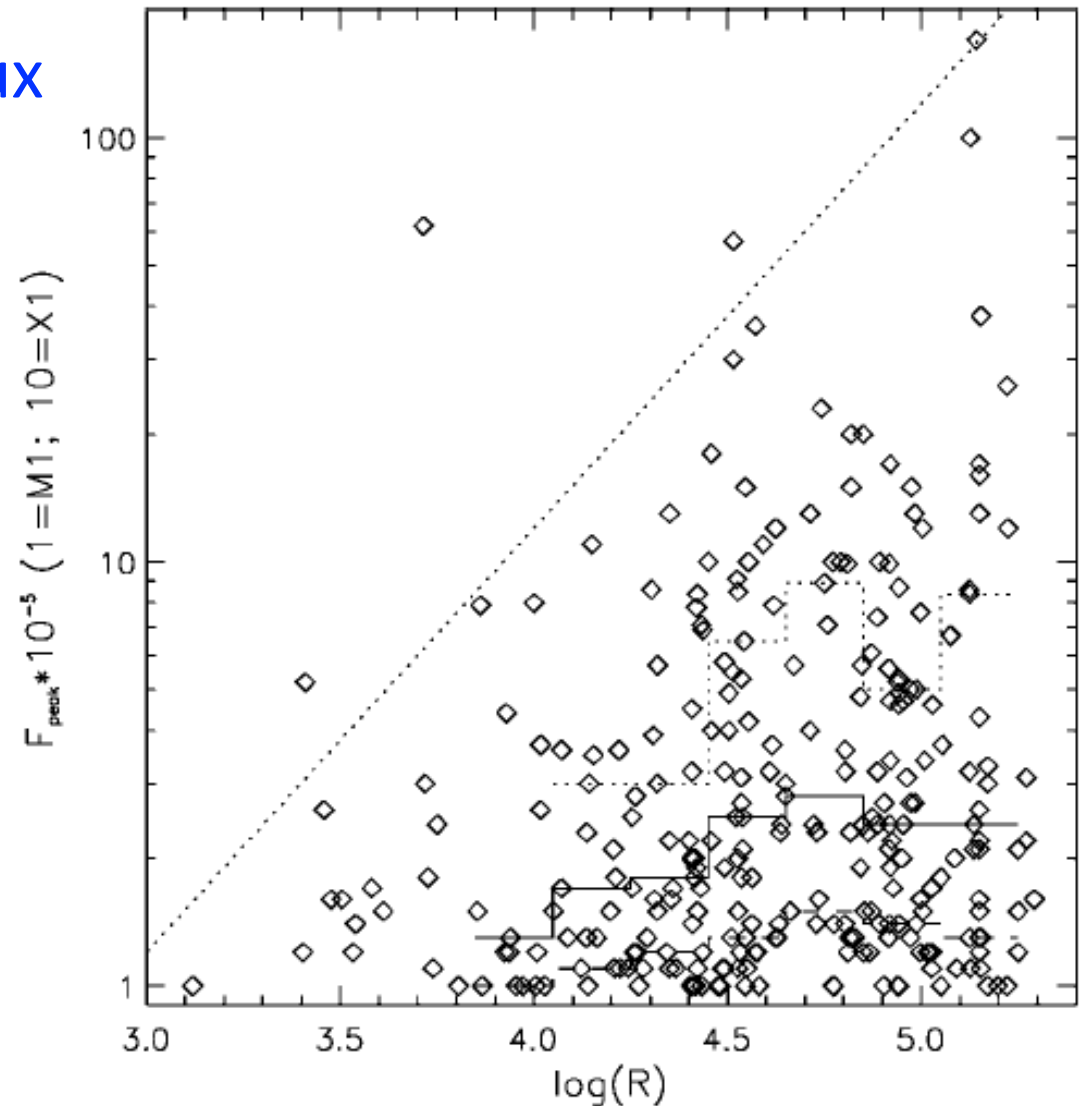
Schrijver (2007) associated large flares with the amount of magnetic flux near strong-field polarity inversion lines (PILs).

$R$  is the total unsigned flux near strong-field PILs



AR 10720 (left) and its masked PILs (right)

$R$  should be strongly correlated with the length of “strong gradient” PILs, which Falconer and collaborators have associated with CMEs.



To relate photospheric magnetic properties to flaring, we must parametrize flare activity.

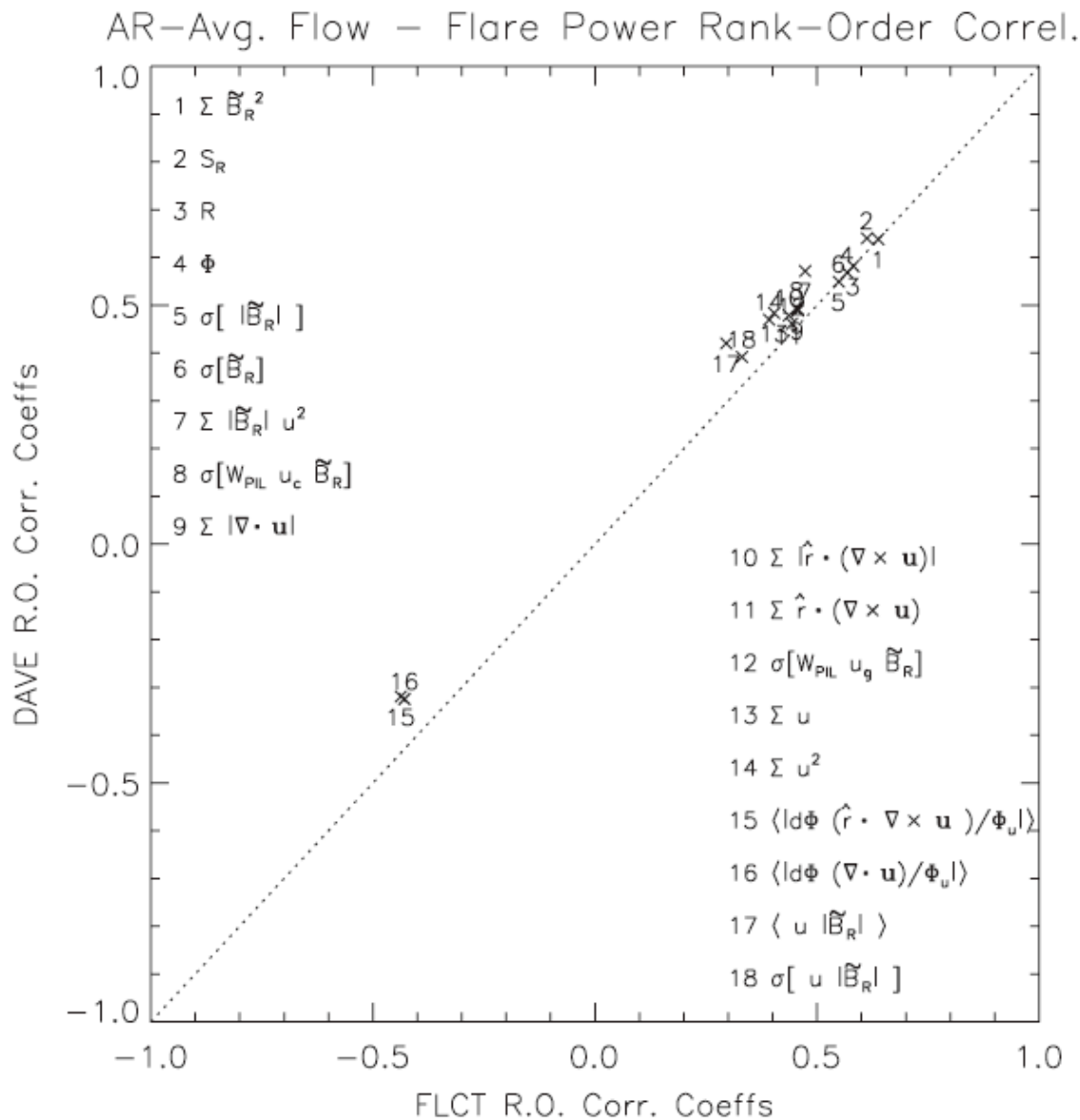
- We binned flares in five time intervals,  $\tau$ :
  - time to cross the region within  $45^\circ$  of disk center (few days);
  - 6C/24C: the 6 & 24 hr windows centered each flow estimate;
  - 6N/24N: the “next” 6 & 24 hr windows after 6C/24C  
(6N is 3-9 hours in the future; 24N is 12-36 hours in the future)
- Following Abramenko (2005), we computed an average GOES flare flux [ $\mu\text{W}/\text{m}^2/\text{day}$ ] for each window:

$$F = (100 S^{(X)} + 10 S^{(M)} + 1.0 S^{(C)}) / \tau ;$$

exponents are summed in-class GOES significands

- Our sample: 154 C-flares, 15 M-flares, and 2 X-flares

Correlation analysis showed several variables associated with average flare flux  $F$ . This plot is for disk-passage averages.

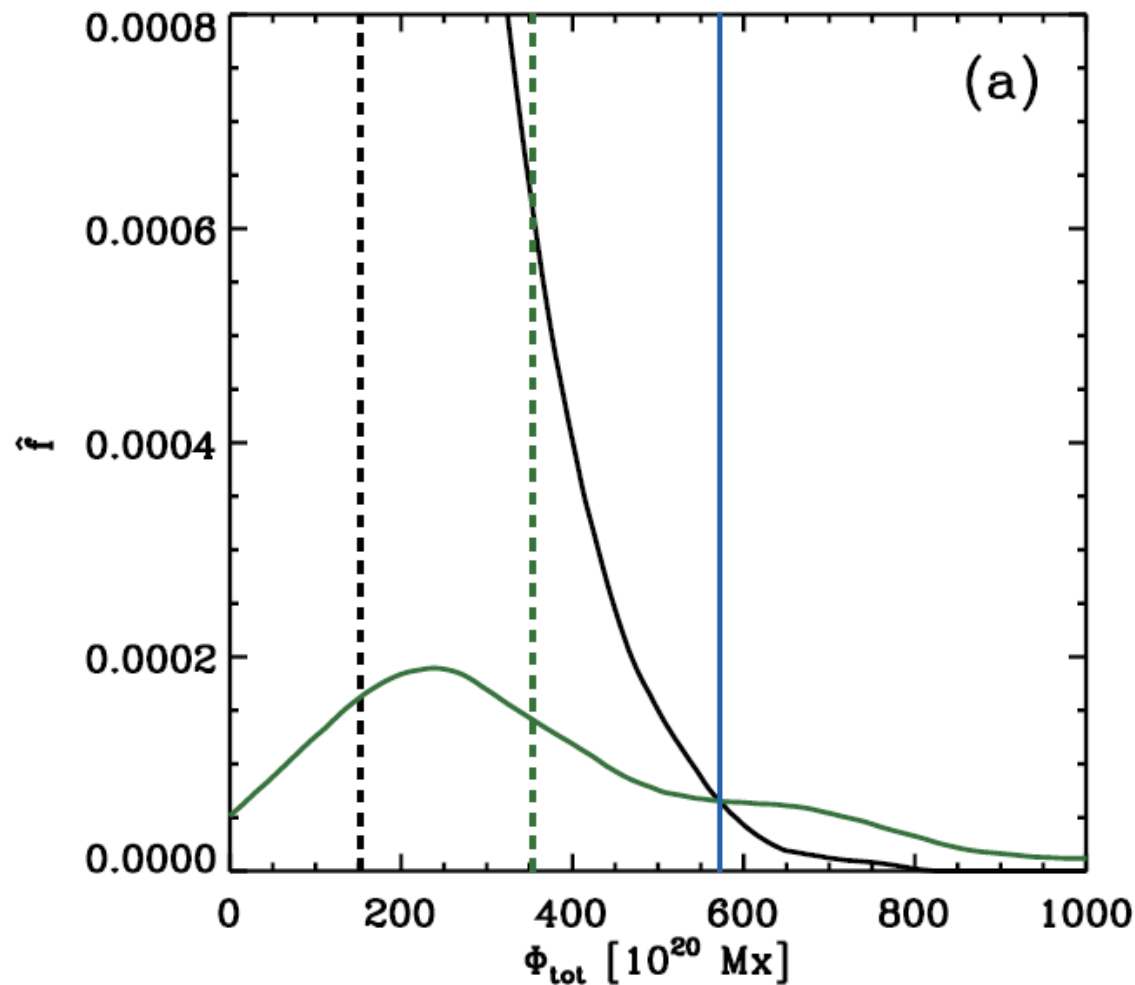


Field and flow properties are ranked by distance from (0,0), the point of complete lack of correlation.

Only the highest-ranked properties tested are shown.

The more FLCT and DAVE correlations agree, the closer they lie to the diagonal line (not a fit).

Discriminant analysis can test the capability of one or more magnetic parameters to predict flares.



1) For one parameter, estimate distribution functions for the flaring (green) and nonflaring (black) populations for a time window  $\Delta t$ , in a “training dataset.”

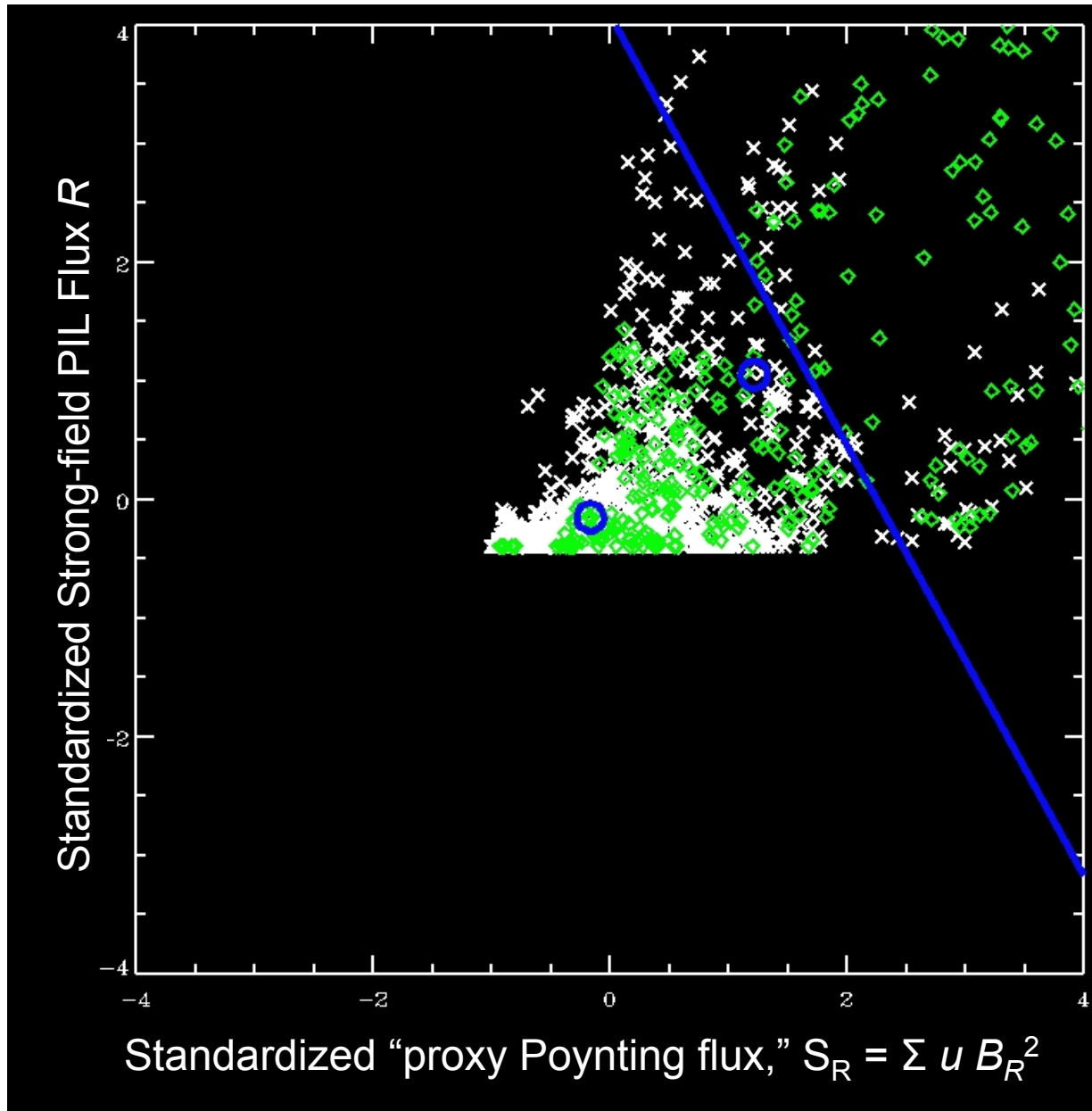
2) Given an observed value  $\mathbf{x}$ , predict a flare within the next  $\Delta t$  if:

$$P_{\text{flare}}(\mathbf{x}) > P_{\text{non-flare}}(\mathbf{x})$$

(vertical blue line)

From Barnes and Leka 2008

Given two input variables, DA finds an optimal **dividing line** between the **flaring** and quiet populations.



Blue circles are means of the **flaring** and non-flaring populations.

The angle of the dividing line can indicate which variable discriminates most strongly.

We paired field/ flow properties "head to head" to identify the strongest flare discriminators.

We used discriminant analysis to pair field/ flow properties “head to head” to identify the strongest flare associations.

Wind.	Variable(s) Considered <sup>a</sup>	[Disc. Coeff.]	PF/F <sup>b</sup>	PNF <sup>c</sup> /F	PF/NF <sup>d</sup>	PNF/NF	<i>SS</i>
6C	$\sum u  \tilde{B}_R ^2$		115	201	96	2296	0.16
6C	$\sum u  \tilde{B}_R ^2$ [1.25], $R$ [1.12]		107	209	64	2328	0.20
6C	$\sum u  \tilde{B}_R ^2$ [0.95], $R$ [1.11], $\langle  \tilde{B}_R  \rangle$ [0.39]		108	208	66	2326	0.21
6N	$R$		39	80	62	2527	-0.08
6N	$R$ [1.96], $\sum u  \tilde{B}_R ^2$ [0.78]		41	78	65	2524	-0.08
6N	$R$ [1.89], $\sum u  \tilde{B}_R ^2$ [0.76], $\dot{R}$ [0.53]		40	79	63	2526	-0.04
24C	$\sum u  \tilde{B}_R ^2$		302	371	74	1961	0.33
24C	$\sum u  \tilde{B}_R ^2$ [1.28], $\langle  \tilde{B}_R  \rangle$ [0.96]		336	337	70	1965	0.37
24C	$\sum u  \tilde{B}_R ^2$ [1.53], $\langle  \tilde{B}_R  \rangle$ [0.88], $\langle \tilde{B}_R \rangle$ [0.48]		354	319	81	1954	0.39
24N	$\sum u  \tilde{B}_R ^2$		118	210	98	2282	0.16
24N	$\sum u  \tilde{B}_R ^2$ [1.43], $R$ [0.67]		115	213	82	2298	0.18
24N	$\sum u  \tilde{B}_R ^2$ [1.45], $R$ [0.40], $\mathcal{F}_{24,\text{current}}$ [0.46]		121	207	72	2308	0.20

For all time windows, **regardless of whether FLCT or DAVE flows were used**, DA consistently ranked  $\sum u B_R^2$  among the two most powerful discriminators.

We found  $R$  and the proxy Poynting flux  $S_R = \Sigma u B_R^2$  to be most strongly associated with flares.

$S_R = \Sigma u B_R^2$  seems to be a robust flare predictor:

- speed  $u$  was only weakly correlated with  $B_R$ ;
- $\Sigma B_R^2$  was independently tested;
- using  $u$  from either DAVE or FLCT gave similar results.

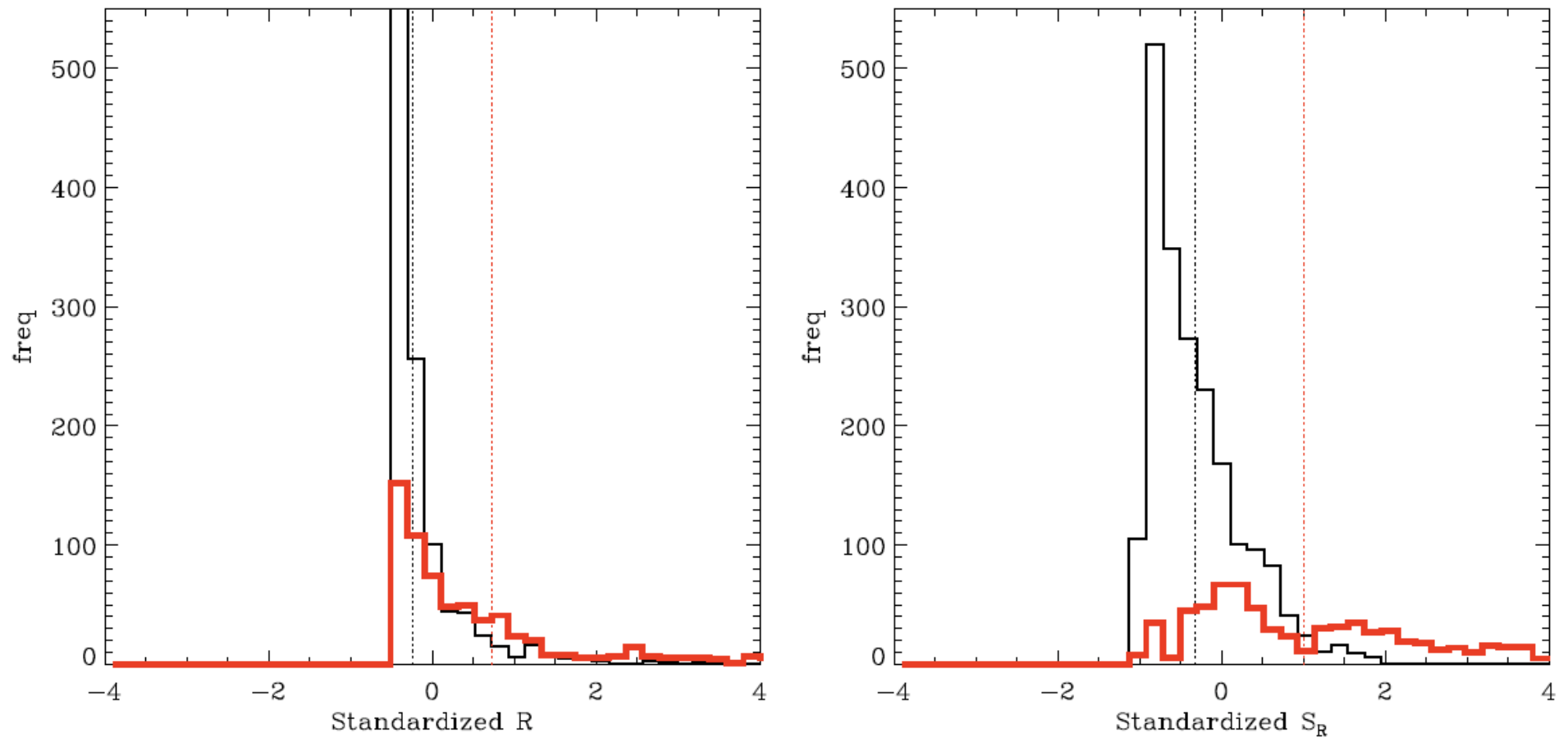
At a minimum, we can say that ARs that are **both** relatively large and rapidly evolving are more flare-prone. (No surprise!)

Much more work remains!

Our results were empirical; we still need to understand the underlying processes.

For more details, see Welsch et al., ApJ v. 705 p. 821 (2009)

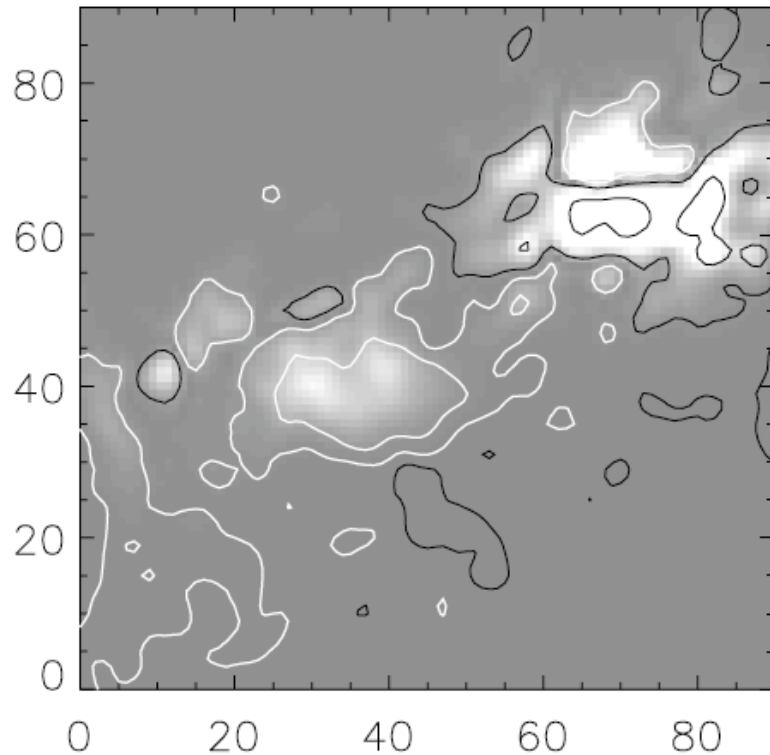
The distributions of flaring & non-flaring observations of  $R$  and  $S_R$  differ, suggesting different underlying physics.



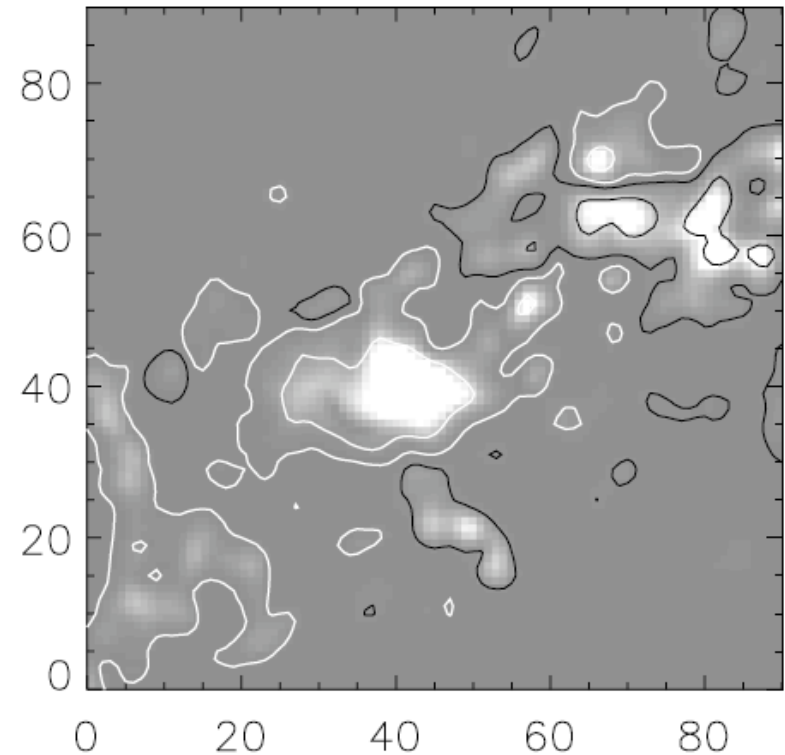
Histograms show non-flaring (black) and flaring (red) observations for  $R$  and  $S_R$  in  $\pm 12$  hr time windows.

Distinct regions contribute to the sums for  $R$  and  $S_R$ , implying different underlying physical processes.

Grayscale Map of SPIL Flux



Grayscale Map of  $u B_R^2$



White regions show strong contributions to  $R$  and  $S_R$  in AR 8100; white/black contours show  $\pm B_R$  at 100G, 500G.

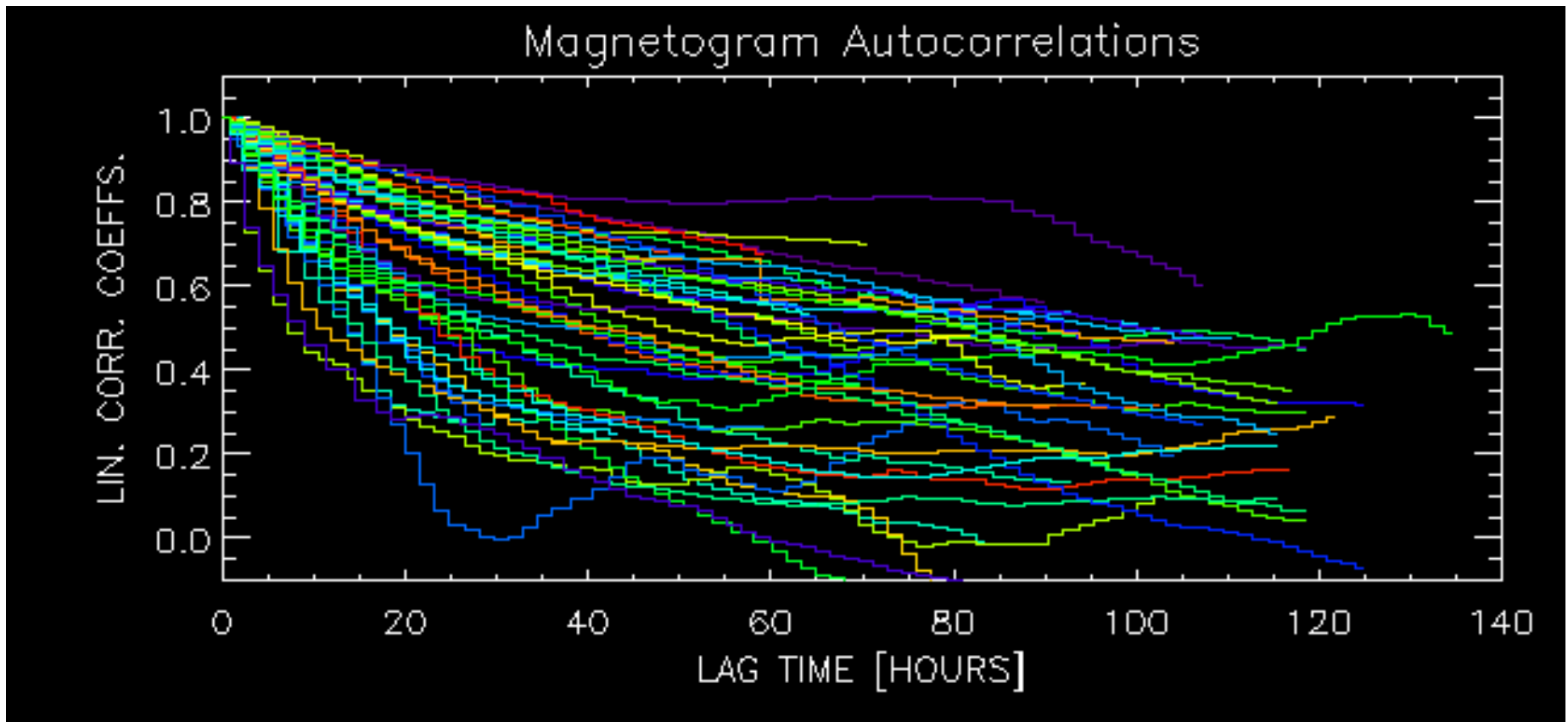
Physically, why is the proxy Poynting flux,  $S_R = \Sigma u B_R^2$ , associated with flaring? Open questions:

- Why should  $u B_R^2$  – part of the horizontal Poynting flux from  $\mathbf{E}_h \times \mathbf{B}_r$  – matter for flaring?
  - The vertical Poynting flux, due to  $\mathbf{E}_h \times \mathbf{B}_h$ , is presumably primarily responsible for injecting energy into the corona.
  - Another component of the horizontal Poynting flux, from  $\mathbf{E}_r \times \mathbf{B}_h$ , was neglected in our analysis. Is it also significant?
- With  $\mathbf{B}_h$  available from HMI and SOLIS vector magnetograms, these questions can be addressed!

Physically, why is the proxy Poynting flux,  $S_R = \Sigma u B_R^2$ , associated with flaring? Open questions, cont'd:

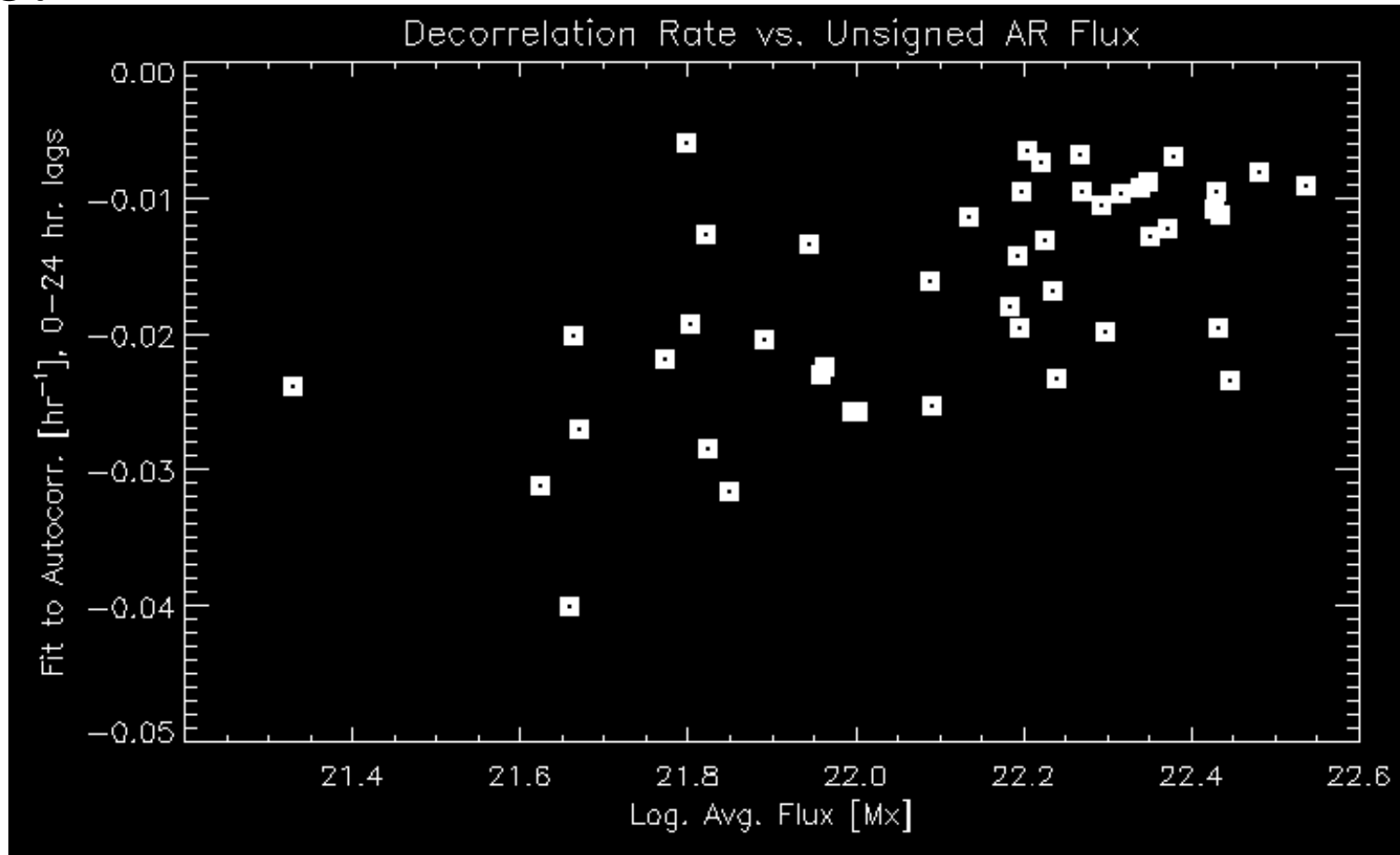
- Do flows from flux emergence or rotating sunspots --- thought to be associated with flares --- also produce large values of  $u B_R^2$ ?
- How is  $u B_R^2$  related to flare-associated subsurface flow properties (e.g., Komm & Hill 2009; Reinard et al. 2010)?

Aside: Is rapid magnetic evolution, by itself, correlated with flare activity?



We computed the current- to- initial frame autocorrelation coefficients for all ARs in our sample.

Aside: We found that rapid magnetic evolution is anti-correlated with  $\Phi$  --- but  $\Phi$  is correlated with flares!



Hence, rapid magnetic evolution, by itself, is anticorrelated with flaring: small ARs don't flare, but evolve most rapidly.

**Recap:** Analysis of **surface** magnetic evolution can help us understand flares and CMEs in the **corona**.

- Using MDI/LOS magnetograms, we found the “proxy Poynting flux,”  $S_R = \Sigma u B_R^2$  to be related to flare activity.
  - It will be interesting to compare the “proxy” Poynting flux with the Poynting flux from vector magnetogram sequences.
- Vector magnetograms from SOLIS and HMI will provide crucial data for future efforts in this area.

... which I'll now describe.

Recently, we have been developing ways to use vector  $\partial_t \mathbf{B}$  (not just  $\partial_t B_z$ ) to estimate  $\mathbf{v}$  or  $\mathbf{E}$ .

- Previous “component methods” derived  $\mathbf{v}$  or  $\mathbf{E}_h$  from the normal component of the ideal induction equation,

$$\Delta B_z / \Delta t = -c [ \nabla_h \times \mathbf{E}_h ]_z = [ \nabla \times (\mathbf{v} \times \mathbf{B}) ]_z$$

- But the vector induction equation can place additional constraints on  $\mathbf{E}$ :

$$\Delta \mathbf{B} / \Delta t = -c (\nabla \times \mathbf{E}) = \nabla \times (\mathbf{v} \times \mathbf{B}),$$

where I assume the ideal Ohm's Law,\* so  $\mathbf{v} \leftrightarrow \mathbf{E}$ :

$$\mathbf{E} = -(\mathbf{v} \times \mathbf{B}) / c \implies \mathbf{E} \cdot \mathbf{B} = 0$$

\*One can instead use  $\mathbf{E} = -(\mathbf{v} \times \mathbf{B}) / c + \mathbf{R}$ , if some model resistivity  $\mathbf{R}$  is assumed. (I assume  $\mathbf{R}$  might be a function of  $\mathbf{B}$  or  $\mathbf{J}$  or ??, but is not a function of  $\mathbf{E}$ .)

The “PTD” method employs a poloidal-toroidal decomposition of  $\mathbf{B}$  into two scalar potentials.

$$\mathbf{B} = \nabla \times (\nabla \times \mathcal{B} \hat{\mathbf{z}}) + \nabla \times J \hat{\mathbf{z}}$$

$$B_z = -\nabla_h^2 \mathcal{B},$$

$$4\pi J_z / c = \nabla_h^2 J,$$

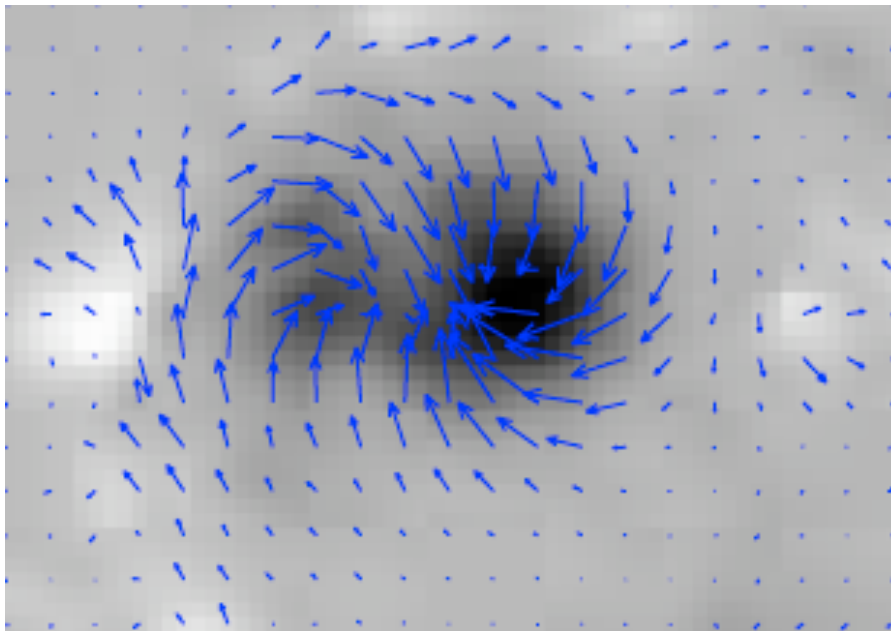
$$\nabla_h \cdot \mathbf{B}_h = \nabla_h^2 (\partial_z \mathcal{B})$$

$$\partial_t \mathbf{B} = \nabla \times (\nabla \times \partial_t \mathcal{B} \hat{\mathbf{z}}) + \nabla \times \partial_t J \hat{\mathbf{z}}$$

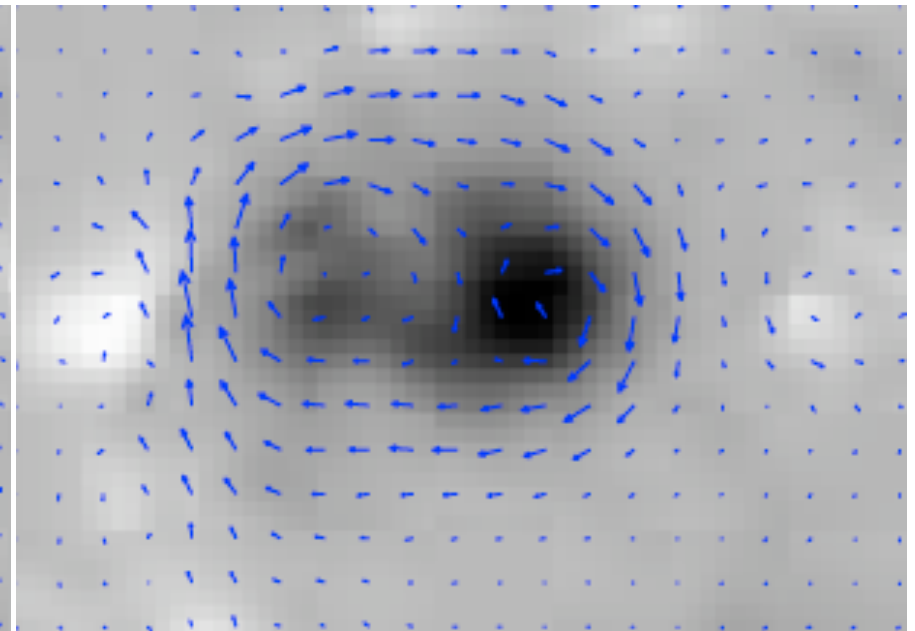
$$\partial_t B_z = \nabla_h^2 (\partial_t \mathcal{B})$$

$$4\pi \partial_t J_z / c = \nabla_h^2 (\partial_t J)$$

$$\nabla_h \cdot (\partial_t \mathbf{B}_h) = \nabla_h^2 (\partial_z (\partial_t \mathcal{B}))$$



Left: the full vector field  $\mathbf{B}$  in AR 8210.



Right: the part of  $\mathbf{B}_h$  due only to  $J_z$ .

Faraday's Law implies that PTD can be used to derive an electric field  $\mathbf{E}$  from  $\partial_t \mathbf{B}$ .

“Uncurling”  $\partial_t \mathbf{B} = -c(\nabla \times \mathbf{E})$  gives  $\mathbf{E}_{\text{PTD}} = (\nabla_h \times \partial_t \mathcal{B} \hat{\mathbf{z}}) + \partial_t J \hat{\mathbf{z}}$

Note:  $\partial_t \mathbf{B}$  doesn't constrain the “gauge”  $\mathbf{E}$ -field  $-\nabla\psi$ ! So:

$$\mathbf{E}_{\text{tot}} = \mathbf{E}_{\text{PTD}} - \nabla\psi$$

Since PTD uses only  $\partial_t \mathbf{B}$  to derive  $\mathbf{E}$ ,  $(\mathbf{E}_{\text{PTD}} - \nabla\psi) \cdot \mathbf{B} = \mathbf{0}$  can be solved to enforce Ohm's Law ( $\mathbf{E}_{\text{tot}} \cdot \mathbf{B} = \mathbf{0}$ ).

(But applying Ohm's Law still does not fully constrain  $\mathbf{E}_{\text{tot}}$ .)

# PTD has two advantages over previous methods for estimating $\mathbf{E}$ (or $\mathbf{v}$ ):

- In addition to  $\partial_t B_z$ , information from  $\partial_t J_z$  is used in derivation of  $\mathbf{E}$ .
- No tracking is used to derive  $\mathbf{E}$ , but tracking methods (ILCT, DAVE4VM) can provide extra info!

For more about PTD,  
see Fisher et al. 2010,  
in ApJ 715 242  
and  
George Fisher's poster  
#401.13

For details of using such methods  
to drive dynamic simulations of the  
corona, see Bill Abbett's poster,  
#405.02

The  $\mathbf{E}$  derived via PTD uses only  $\partial_t \mathbf{B}$ , so  $\mathbf{E}_{\text{PTD}} \cdot \mathbf{B} \neq \mathbf{0}$ .  
Hence, we must solve for  $\psi(x,y)$  so  $(\mathbf{E}_{\text{PTD}} - \nabla\psi) \cdot \mathbf{B} = \mathbf{0}$ .

We have developed a practical iterative approach:

1. Define  $\mathbf{b}$  = unit vector along  $\mathbf{B}$
2. Define  $\nabla\psi = s_1(x, y) \mathbf{b} + s_2(x, y)(\hat{\mathbf{z}} \times \mathbf{b}) + s_3(x, y) \mathbf{b} \times (\hat{\mathbf{z}} \times \mathbf{b})$
3. Set  $s_1(x, y) = \mathbf{E}_{\text{PTD}} \cdot \mathbf{b}$
4. Solve  $\nabla_h^2 \psi = \nabla_h \cdot [s_1(x, y) \mathbf{b}_h + s_2(x, y)(\hat{\mathbf{z}} \times \mathbf{b}) - s_3(x, y) \mathbf{b}_z \mathbf{b}_h]$
5. Update  $s_2 = \hat{\mathbf{z}} \cdot (\mathbf{b}_h \times \nabla\psi) / b_h^2$  and  $s_3 = \partial_z \psi - (\mathbf{b}_h \cdot \nabla\psi) b_z / b_h^2$
6. Repeat steps 4 & 5 until convergence.

This approach quickly yields a solution.

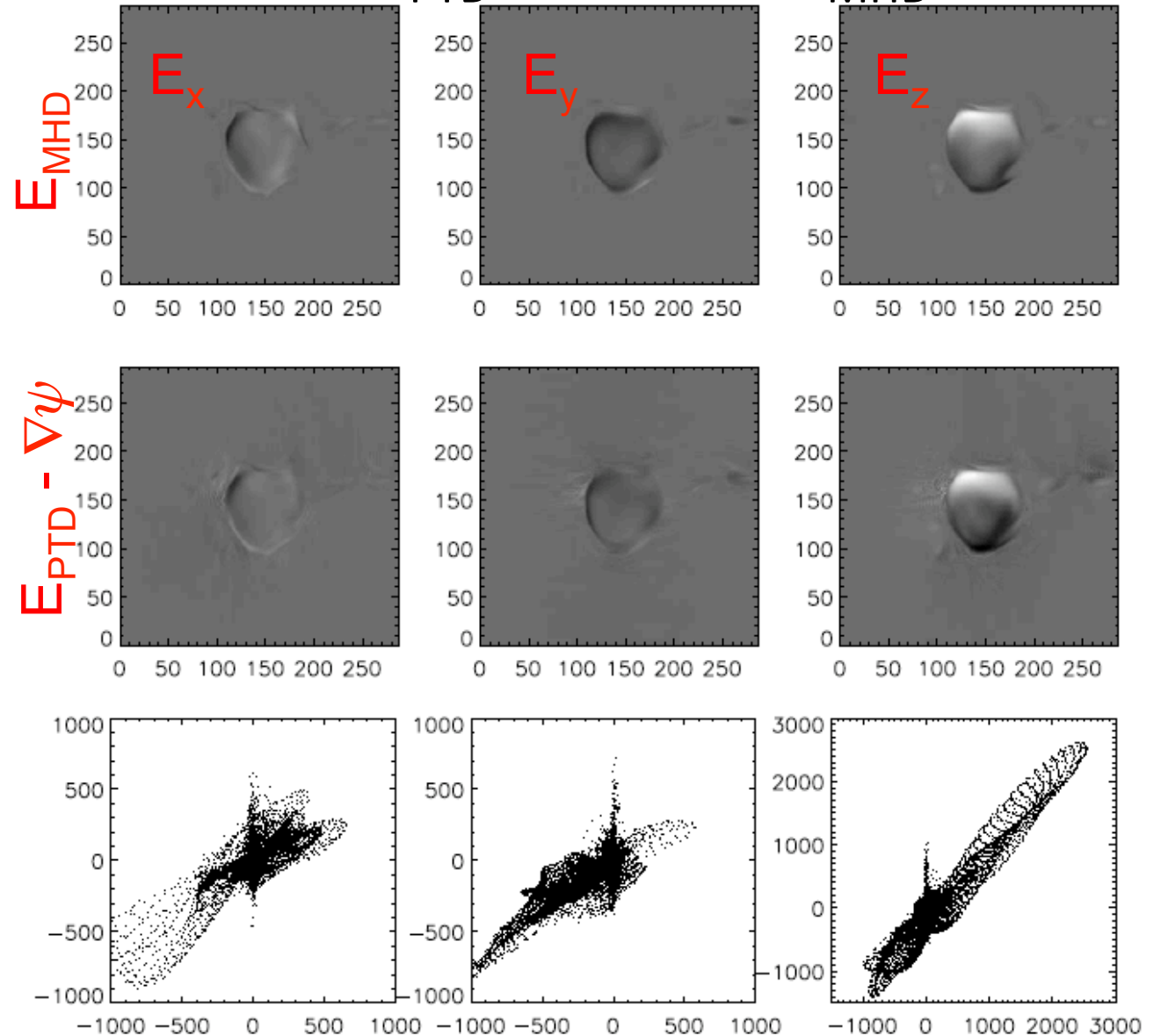
However, uniqueness is still a problem: any  $\nabla\psi(x,y)$  satisfying  $\nabla\psi \cdot \mathbf{B} = \mathbf{0}$  can be added to this solution!

For (many) more details about PTD, see Fisher et al. 2010.

How accurate is PTD? We used data from MHD simulations to compare  $\mathbf{E} = \mathbf{E}_{\text{PTD}} - \nabla\psi$  with  $\mathbf{E}_{\text{MHD}}$ .

Synthetic data were those used by Welsch et al. (2007) to test tracking methods.

The PTD + iteration solution was more accurate than most other methods tested by Welsch et al. (2007).



While  $\partial_t \mathbf{B}$  provides more information about  $\mathbf{E}$  than  $\partial_t B_z$  alone, it still does not fully determine  $\mathbf{E}$ .

1. Faraday's Law only relates  $\partial_t \mathbf{B}$  to the curl of  $\mathbf{E}$ , not  $\mathbf{E}$  itself; the gauge electric field  $\nabla\psi$  is unconstrained by  $\partial_t \mathbf{B}$ .

(We used Ohm's Law as an additional constraint.)

2.  $\partial_t \mathbf{B}_h$  also depends upon vertical derivatives in  $\mathbf{E}_h$ , which single-height magnetograms do not fully constrain.

- Additional observational data must be used to obtain more information about both of these unknowns.

Both vector and component methods of finding  $\mathbf{E}$  are underdetermined: unknowns exceed knowns by one!

Method	Unknowns	Knowns
Component Methods	$E_x, E_y, E_z$	$\partial_t B_z, \mathbf{E} \cdot \mathbf{B} = 0$
PTD	$E_x, E_y, E_z, \partial_z E_x, \partial_z E_y$	$\partial_t B_x, \partial_t B_y, \partial_t B_z, \mathbf{E} \cdot \mathbf{B} = 0$

Hence, extra information about  $\mathbf{E}$  provides useful constraints!

1. The flow  $\mathbf{u}$  estimated by tracking can constrain the gauge electric field  $\psi$ , since  $\nabla_h^2 \psi = (\nabla_h \times \mathbf{u} B_z) \cdot \hat{\mathbf{z}}$
2. Where  $B_{\text{LOS}} = 0$ , Doppler shifts can constrain  $\mathbf{E}$ .
3. Magnetograms from multiple heights can constrain  $\partial_z \mathbf{E}_h$ .

(Given noise in the data, overdetermining  $\mathbf{E}$  is fine!)

1. Tracking with “component methods” constrains  $\psi$  by estimating  $\mathbf{u}$  in the source term  $(\nabla_h \times \mathbf{u} \cdot \hat{\mathbf{B}}_z) \cdot \mathbf{z}$ .

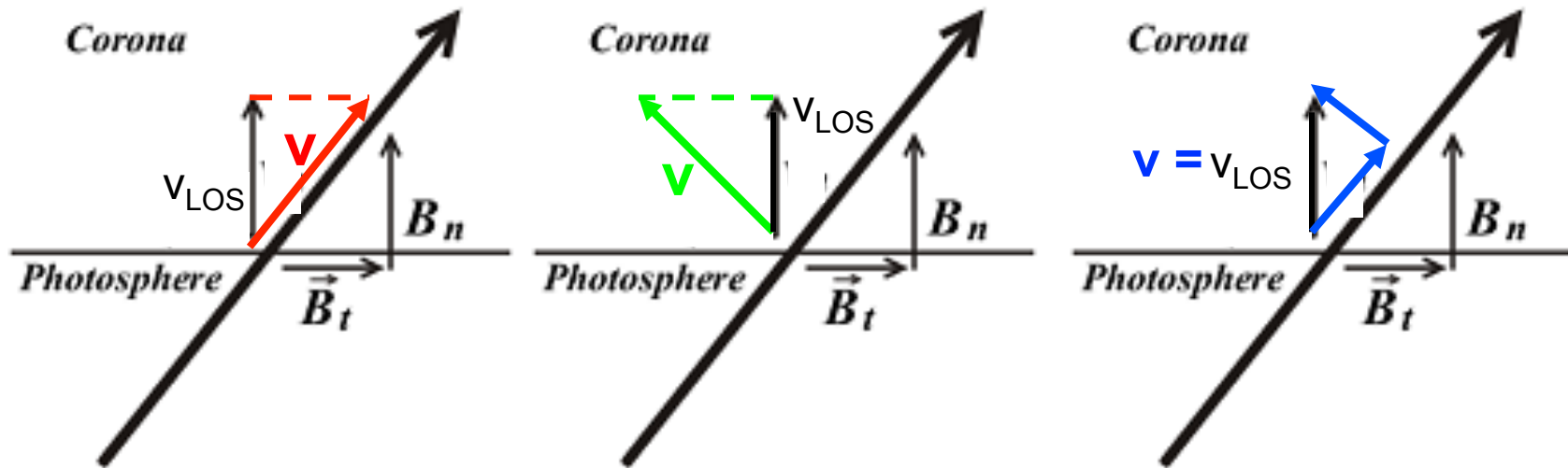
Methods to find  $\psi$  via tracking include, e.g.:

- Local Correlation Tracking (**LCT**, November & Simon 1988; **ILCT**, Welsch et al. 2004; **FLCT** Fisher & Welsch 2008)
- the Differential Affine Velocity Estimator (**DAVE**, and **DAVE4VM**; Schuck 2006 & Schuck 2008)

(Methods to find  $\psi$  via integral constraints also exist, e.g., Longcope’s [2004] Minimum Energy Fit [**MEF**] method.)

Welsch et al. (2007) tested some of these methods using “data” from MHD simulations; MEF performed best. Further tests with more realistic data are underway.

2. Flows  $v_{\parallel}$  along  $\mathbf{B}$  do not contribute to  $\mathbf{E} = -(\mathbf{v} \times \mathbf{B})/c$ , but do “contaminate” Doppler measurements.

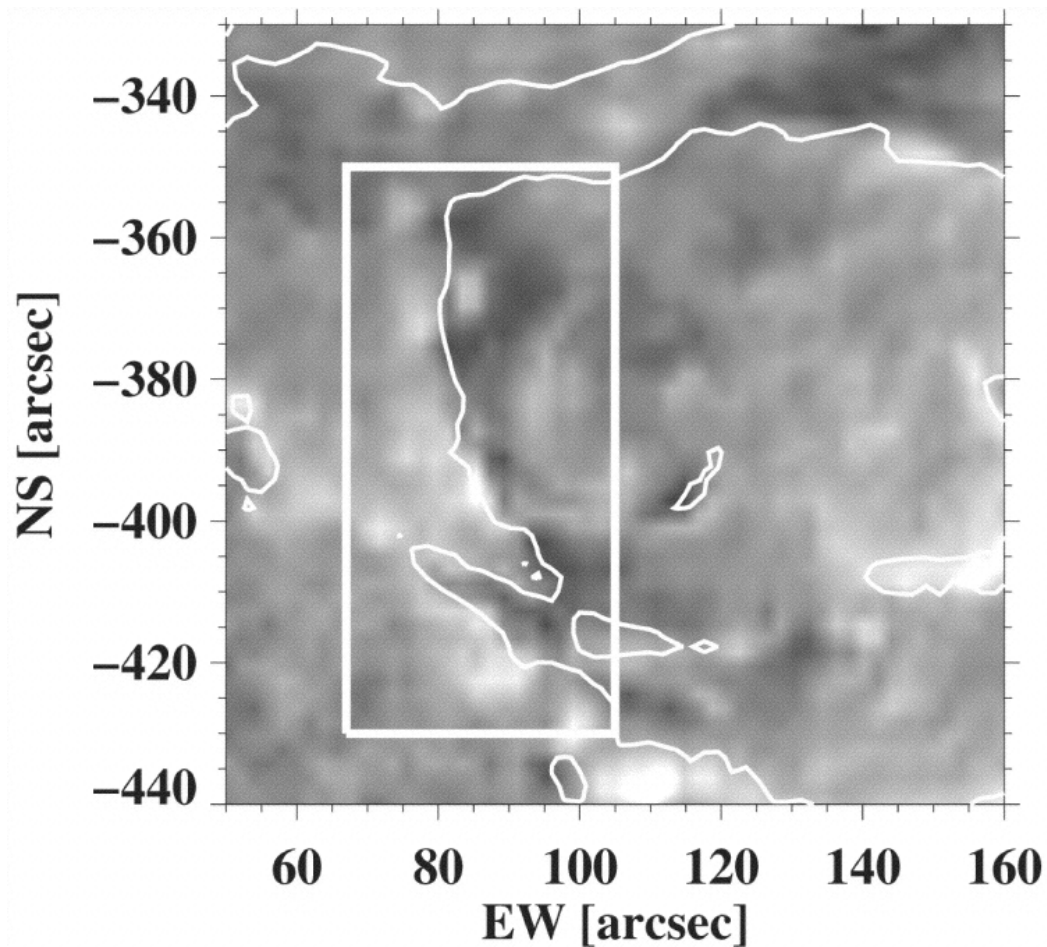


Generally, Doppler shifts cannot distinguish flows parallel to  $\mathbf{B}$  (red), perpendicular to  $\mathbf{B}$  (green), or in an intermediate direction (blue).

With  $\mathbf{v}_{\perp}$  estimated another way & projected onto the LOS, the Doppler shift determines  $v_{\parallel}$  (Georgoulis & LaBonte 2006).

Doppler shifts are only unambiguous along polarity inversion lines (PILs), where  $B_n$  changes sign (Chae *et al.* 2004, Lites 2005).

**Aside:** Dopplergrams are sometimes consistent with “siphon flows” moving along B.



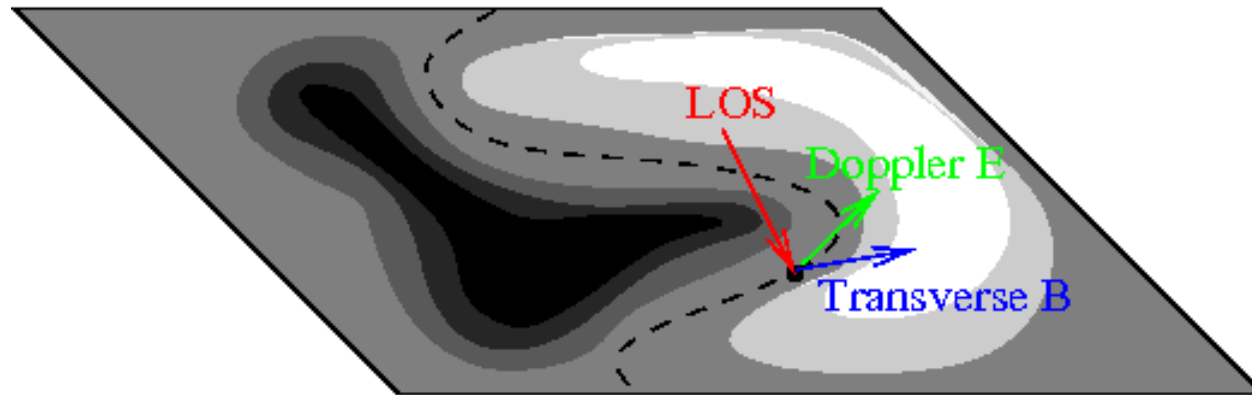
MDI Dopplergram at 19:12 UT on 2003 October 29 superposed with the magnetic polarity inversion line. (From Deng et al. 2006)

Why should a polarity inversion line (PIL) also be a velocity inversion line (VIL)?

One plausible explanation is siphon flows arching over (or ducking under) the PIL.

What's the DC Doppler shift along this PIL? Is flux emerging or submerging?

2. (cont'd) Doppler shifts along PILs of the LOS magnetic field  $B_{\text{LOS}}$  can constrain the ideal electric field  $\mathbf{E}$ .

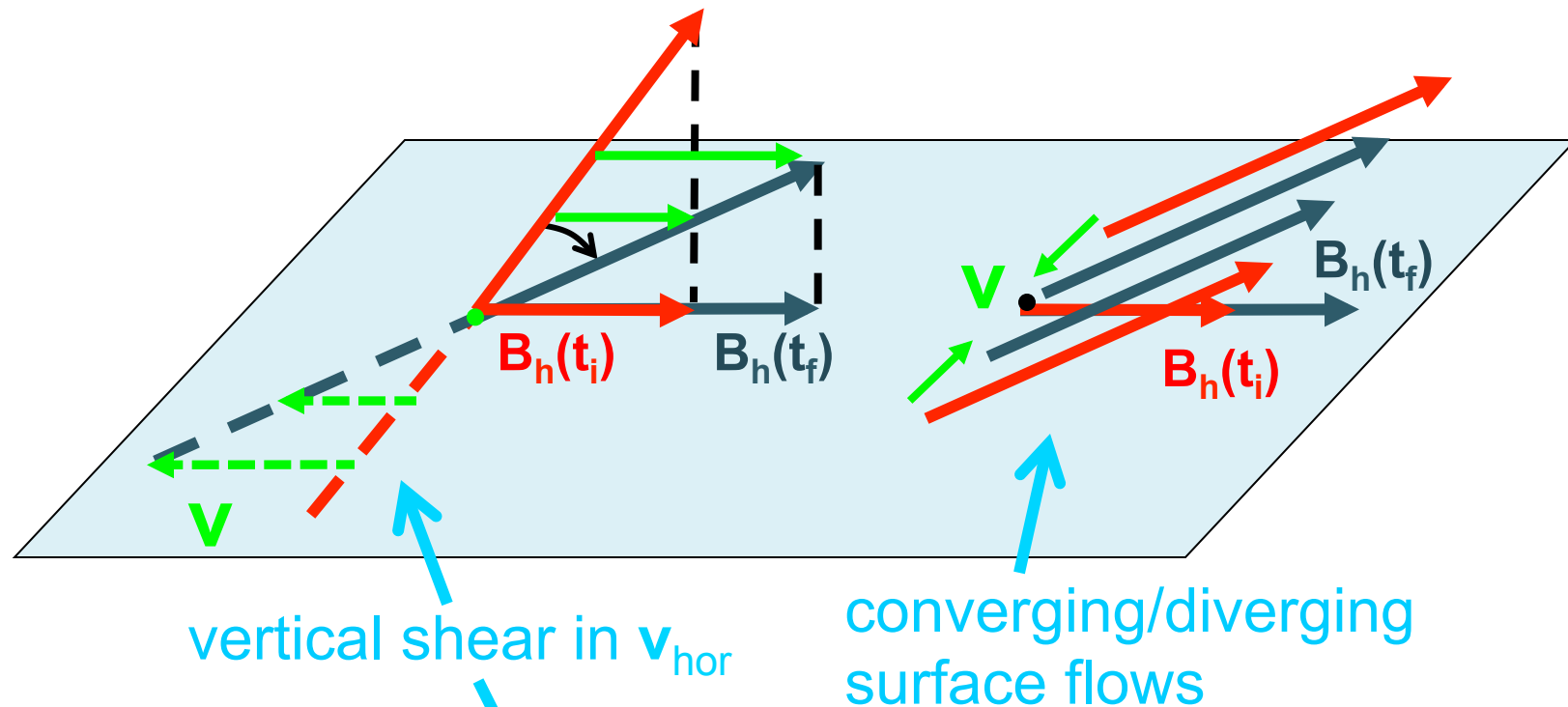


Measurements of  $v_{\text{Dopp}}$  and  $\mathbf{B}_{\text{trans}}$  on PILs are direct observations of the ideal  $\mathbf{E}$  perpendicular to both.

How do PTD  $\mathbf{E}$ -fields compare with measurements of this “Doppler electric field”  $\mathbf{E}_{\text{Dopp}}$ ?

The gradient of a scalar potential  $\psi$  derived from  $\mathbf{E}_{\text{Dopp}}$  can be added to PTD  $\mathbf{E}$ -fields to improve consistency.

3. Horizontal flows with either vertical shear or nonzero horizontal divergence (or both) alter the horizontal field  $\mathbf{B}_h$ .



$$\partial_t \mathbf{B}_h = \partial_z (\mathbf{E}_h \times \hat{\mathbf{z}}) - \underbrace{(\nabla_h \times \mathbf{E}_z \hat{\mathbf{z}})}$$

If only vertical shear causes  $\partial_t \mathbf{B}_h$ , then  $\mathbf{E}_h = 0$ , and there is no vertical Poynting flux!

$\partial_z \mathbf{E}_h$  estimated from magnetograms at different heights (e.g., HMI + SOLIS, or HMI + Hinode) can constrain which process is at work.

# Summary

Studying photospheric magnetic evolution is clearly necessary to understand how flares and CMEs work.

Our methods of quantitatively characterizing magnetic evolution are promising tools to address this challenge!

Improvements in the quality and coverage of vector magnetogram data from NSO's SOLIS and SDO/ HMI should help us learn more in the coming years!



*A copy of this talk is available online at:*

*<http://solarmuri.ssl.berkeley.edu/~welsch/brian/public/presentations/HarveyPrize/>*

# Acknowledgements



I've been very lucky to work with George Fisher (left), my post-doc advisor and current "boss" (note quotes!), and Dana Longcope (right), my PhD advisor.



***Thank you both for all you've taught me!***

Many other friends and colleagues have supported me in my career, but I don't have time to name them all.

To each of you: ***Thank you!***

The ideal induction equation is:

$$\begin{aligned}\partial_t \mathbf{B}_x &= (-\partial_y E_z + \partial_z E_y) c \\ &= \partial_y (v_x B_y - v_y B_x) - \partial_z (v_z B_x - v_x B_y)\end{aligned}$$

$$\begin{aligned}\partial_t \mathbf{B}_y &= (-\partial_z E_x + \partial_x E_z) c \\ &= \partial_z (v_y B_z - v_z B_y) - \partial_x (v_x B_y - v_y B_x)\end{aligned}$$

$$\begin{aligned}\partial_t \mathbf{B}_z &= (-\partial_x E_y + \partial_y E_x) c \\ &= \partial_x (v_z B_x - v_x B_z) - \partial_y (v_y B_z - v_z B_y)\end{aligned}$$